REVIEW

Deep impurity-center ionization by far-infrared radiation

S. D. Ganichev* and W. Prettl

Institut für Angewandte Physik, Universität Regensburg, D-93040 Regensburg, Germany,

I. N. Yassievich

A. F. Ioffe Physicotechnical Institute, Russian Academy of Sciences, 194021 St. Petersburg, Russia
(Submitted April 21, 1997)
Fiz. Tverd. Tela (St. Petersburg) **39**, 1905–1932 (November 1997)

An analysis is made of the ionization of deep impurity centers by high-intensity far-infrared and submillimeter-wavelength radiation, with photon energies tens of times lower than the impurity ionization energy. Within a broad range of intensities and wavelengths, terahertz electric fields of the exciting radiation act as a dc field. Under these conditions, deep-center ionization can be described as multiphonon-assisted tunneling, in which carrier emission is accompanied by defect tunneling in configuration space and electron tunneling in the electric field. The field dependence of the ionization probability permits one to determine the defect tunneling times and the character of the defect adiabatic potentials. The ionization probability deviates from the field dependence $e(E) \propto \exp(E^2/E_c^2)$ (where E is the wave field, and E_c is a characteristic field) corresponding to multiphonon-assisted tunneling ionization in relatively low fields, where the defects are ionized through the Poole–Frenkel effect, and in very strong fields, where the ionization is produced by direct tunneling without thermal activation. The effects resulting from the high radiation frequency are considered and it is shown that, at low temperatures, they become dominant. © *1997 American Institute of Physics.* [S1063-7834(97)00111-1]

INTRODUCTION

The interest in the spectroscopy of semiconductors and semiconductor structures in the far-infrared (FIR) and submillimeter (SBM) ranges (wavelengths extending from 30 to 1000 μm, corresponding to photon energies from 35 to 1 meV) is stimulated primarily by the fact that they include the characteristic energies of many elementary excitations in semiconductors. Among these are the plasma oscillation energy, the ionization energies of typical shallow donors and acceptors, the cyclotron and spin interaction energies, the characteristic size-quantization energies of the electron subsystem, optical phonon energies etc. For many decades the FIR and SBM ranges have been among the hardest to access experimentally. The advent of novel radiation sources in the recent twenty to thirty years has made possible a large number of experiments making use of grating monochromators, Fabry–Perot interferometers, backward-wave tubes, and relatively lower-power, electrically or optically pumped cw lasers emitting discrete lines. SBM and FIR spectroscopy has become an efficient tool in studies of material properties and of the various phenomena in different areas of research. The appearance of high-power pulsed FIR and SBM lasers (first of the TEA CO_2-pumped, molecular-gas type[1,2] and, subsequently, of free-electron lasers[3,4] and p-Ge semiconductor devices[5–10]) capable of delivering nanosecond pulses of high intensity, up to a few MW, has opened up totally new vistas in investigation of semiconductors in the FIR range and provided a basis for development of far-infrared spectroscopy of semiconductors at high excitation levels, which was first made use of at the Ioffe Physicotechnical Institute.[11]

In this frequency range, the high radiation intensity gives rise to a variety of nonlinear phenomena in semiconductors and semiconductor structures (see, e.g., review[12]), such as, for example, multiphoton absorption,[13–19] absorption saturation (bleaching),[20–30] nonlinear cyclotron resonance,[31,32] impact ionization,[33,34] nonlinear photoacoustic spectroscopy,[35] high-harmonic generation,[36,37] and the high-frequency Stark effect,[38] whose characteristics differ substantially from their counterparts observed both in the visible and infrared ranges and in the range extending from microwaves to dc electric fields. The reason for this lies in that the FIR–SBM range is actually a domain where the interaction in the electron-photon system undergoes a transition from the quantum to classical limit, thus creating a unique possibility to study the same physical phenomenon in conditions where by properly varying the frequency or intensity of radiation one can make dominant either the discrete properties of light or its wave characteristics. Submillimeter and far-infrared spectroscopy at high-excitation levels has also an essential advantage in that it makes a technique more sensitive due to the high intensity of radiation, i.e. to the larger number of photons. Since the photon energy is here much less than the gap width and, hence, there can be no direct one-photon generation of free carriers, observation of the relatively weak effects of carrier redistribution in momentum and energy becomes possible. The high radiation intensity permits one also to study in detail such photoelectric phenomena as, for instance, the

linear and nonlinear electron-gas heating,[21,29,33,34,39–44] photoelectric phenomena associated with Bloch oscillations,[45,46] photon drag of electrons,[11,15,47–52] photogalvanic effect,[53–57] photoresistive effects produced in semiconductor structures in plasma reflection,[58–62] and multiphoton resonant tunneling in quantum-well structures,[18] as well as to use them in development of radiation detectors.[47,50,51,63–68]

This work deals with the new nonlinear effect of deep-impurity ionization by FIR radiation at photon energies a few tens of times lower than the impurity binding energy reported in Ref. 69. We are going to consider impurity centers with no direct coupling of light to localized vibrational modes. The ionization process is studied by the photoconductivity method,[70] which is traditionally used in optical research and is capable of detecting extremely small ($<0.01\%$) changes in carrier concentration, thus providing a high measurement sensitivity.

If there are no free carriers in the semiconductor, deep impurities can be ionized through tunneling in the strong electric field of the radiation. In most cases, the FIR radiation acts here as a strong dc electric field, and the ionization probability does not depend on the radiation frequency. An increase of the frequency and decrease of temperature result in the ionization probability becoming dependent on frequency, which signals the transition to the case when the magnitude of the photon energy becomes significant.

Deep impurity centers play a dominant part in the electronic properties of semiconductor materials and have therefore become a subject of extensive investigation.[71–77] It is the deep centers that determine usually the nonequilibrium carrier lifetimes by acting as centers of nonradiative recombination and thermal ionization. Investigation of the effect of electric field on thermal ionization and carrier trapping has been traditionally used to probe deep impurities. In particular, investigation of the ionization or capture in a strong electric field is actually the only way to find the parameters of the multiphonon transitions determining the nonradiative recombination rate. Deep-level transient spectroscopy (DLTS) is also among the most extensively employed tools. Most of the deep-center parameters (ionization energy, nonradiative and radiative trapping cross sections) were obtained using various modifications of DLTS. It should be noted, however, that nonuniformities of the electric field in a structure make interpretation of the results obtained difficult. Direct application of strong static electric fields is usually complicated by the onset of field nonuniformities in the sample and quite frequently initiates avalanche breakdown. Using the electric field of high-intensity, short laser pulses in the far-infrared range at THz frequencies avoids such problems and permits contactless and uniform application of strong electric fields. Despite the high radiation intensities involved, there is none or only insignificant heating of the electron gas or of the crystal lattice under these conditions. This is the result of the extremely weak absorption of the FIR radiation due to the low concentration of free carriers (the carriers are frozen out on the centers), as well as to the use of short, nanosecond-range pulses, which do not perturb substantially the phonon system.

Thus discovery of multiphonon tunneling ionization under contactless application of a strong uniform electric field and using short radiation pulses with duration shorter than the nonequilibrium carrier lifetimes has permitted development of a new method for probing deep impurity centers in semiconductors, offering a possibility of determining the multiphonon parameters of deep-level impurities, the structure of their adiabatic potentials, and the trapping kinetics of nonequilibrium carriers.

The present review deals with the ionization of deep impurity centers by high-intensity, pulsed FIR–SBM radiation. Section 1 considers the theory of deep-impurity ionization by a dc and high-frequency electric field, Sec. 2 discusses the experimental techniques used and subjects of investigation, Sec. 3 analyzes the conditions under which one observes tunneling ionization and considers other possible mechanisms, Sec. 4 presents and discusses in detail the relevant experimental results, Sec. 5 looks into the application of the method of multiphonon impurity ionization by FIR–SBM radiation to studies of relaxation dynamics in the particular case of the trapping kinetics of nonequilibrium carriers in GaP:Te, and Sec. 6 sums up the review with main conclusions. The Appendix includes effects of linear and nonlinear electron-gas heating by far-infrared radiation, and it shows that these phenomena do not play a significant role in the experiments discussed here.

1. DEEP-IMPURITY IONIZATION BY AN ELECTRIC FIELD

1.1. Adiabatic approximation

The binding energy of deep centers exceeds by far the average phonon energy, and therefore only multiphonon-assisted processes can give rise to thermal emission. Since electronic transitions occur much faster than transitions in the phonon system, one can use the adiabatic approximation in the description of electron-phonon interaction.[78]

Consider the simplest case of the deep impurity having only one bound state. Obviously enough, this model is directly applicable to the capture by neutral centers, and, as this will be shown in Sec. 1.5, the main conclusions reached here remain valid also for deep attractive centers. The position of the localized level is determined by the potential generated by the impurity and is substantially dependent on the distance from the impurity to the nearest atoms. Thus vibrations of the impurity and of the lattice modulate the position of the localized electronic level, as this is shown in Fig. 1. Strong thermal vibrations can eventually drive the level to continuum, thus producing ionization of the impurity.[79] Quantitative consideration is usually made using a single-mode model, which describes the impurity vibrations through variation of only one configuration coordinate x. This approximation is valid, because the multiphonon ionization of deep impurities and the trapping by the latter are dominated by the breathing mode of localized vibrations. The adiabatic approximation treats electronic transitions as occurring at a fixed configuration coordinate x, with the vibrations of the impurity itself being determined by the potential, which is generated by the surrounding atoms, with due inclusion of the mean polarization field induced by the localized electron. Such potential averaged over electronic

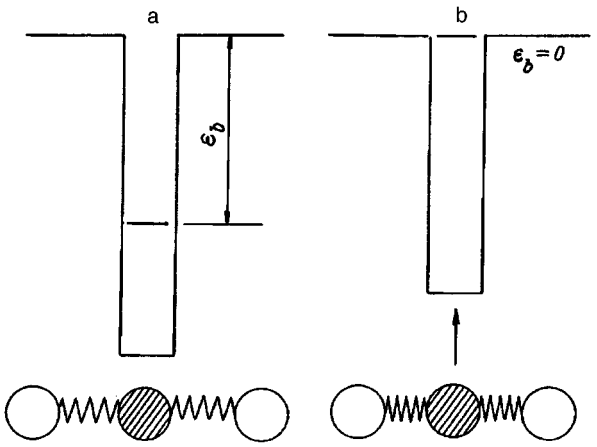

FIG. 1. Modulation of a localized electronic level by the vibrating impurity and lattice. a) ground-state bound electron, vibrational system of the defect in equilibrium; b) defect vibrational system perturbed, the electronic level approaches the continuum.

motion is called adiabatic, and it includes the electron energy at a fixed coordinate x.

Figure 2 shows two main possible configuration-coordinate diagrams: (a) for the case of weak electron-phonon coupling and (b) for strong electron-phonon interaction, where self-trapping occurs, as is the case, for example, with DX and EL2 centers in III-V semiconductors. The potential curve $U_1(x)$ corresponds to the case of the electron bound to the impurity, and $U_2(x)$, to that of an ionized impurity and a free electron with zero kinetic energy. The energy separating the two potentials is determined by the electron binding energy $\varepsilon_b(x)$ at a fixed configuration coordinate x:

$$U_1(x)=U_2(x)-\varepsilon_b(x). \tag{1}$$

The equilibrium positions of the ground state (with the electron bound to the impurity) and the ionized state are shifted with respect to one another as the result of electron-phonon coupling. Accordingly, the optical-ionization energy, by the Franck–Condon principle, can be written as $\varepsilon_{\text{opt}}=\varepsilon_b(x=x_0)$, where x_0 is the equilibrium value of the ground-state configuration coordinate. As seen from Fig. 2, the energy of optical ionization is larger than that of thermal ionization ε_T. The relaxation energy $\Delta\varepsilon=\varepsilon_{\text{opt}}-\varepsilon_T$ characterizes the electron-phonon coupling strength, since the stronger is the coupling, the larger is $\Delta\varepsilon$. The electron-phonon coupling can be conveniently characterized by a dimensionless parameter

$$\beta=\frac{\Delta\varepsilon}{\varepsilon_T}. \tag{2}$$

The configuration of Fig. 2a corresponds to weak electron-phonon coupling ($\beta<1$), and the difference between ε_{opt} and ε_T is, as a rule, small. Actually, no difference has thus been observed between ε_{opt} and ε_T in germanium and sili-

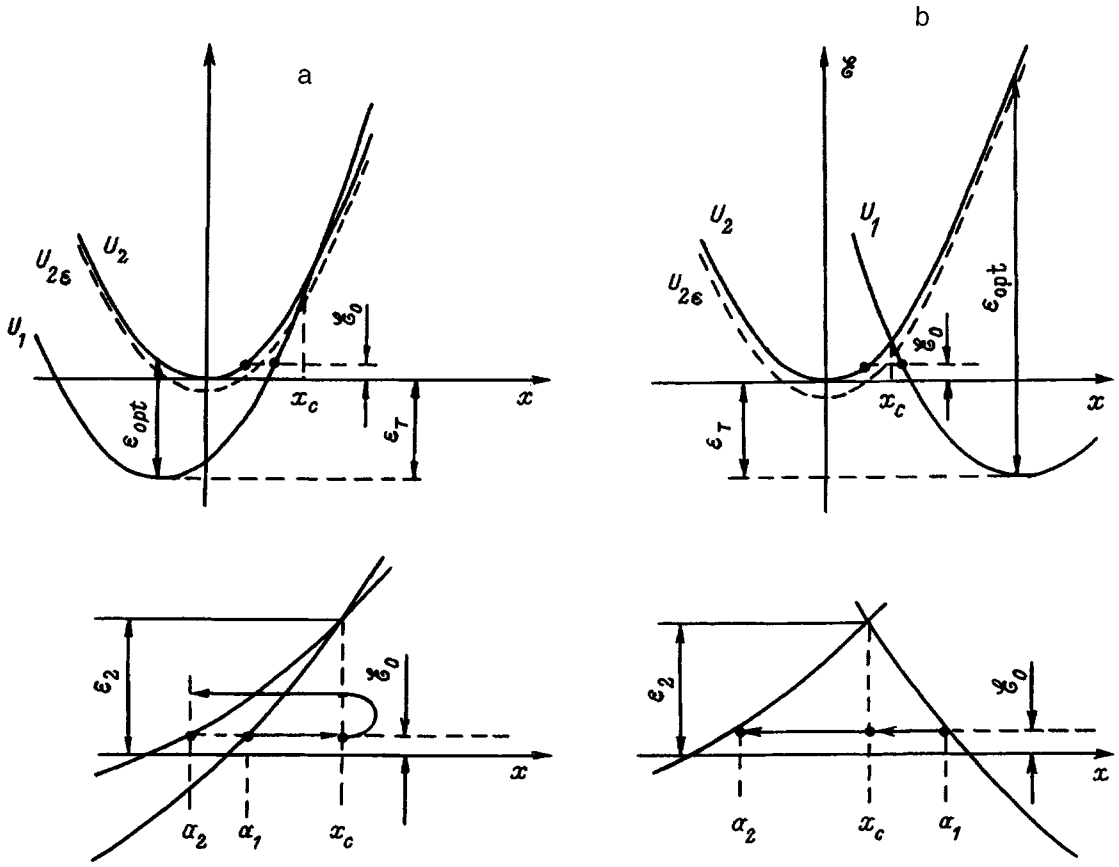

FIG. 2. Two main possible configurational diagrams. a. weak electron-phonon coupling, b. strong electron-phonon coupling allowing self-trapping, as is the case, for instance, with DX centers in III-V semiconductors. Shown below are the tunneling trajectories on an enlarged scale.

con. There are, however, cases, where the relaxation energy is fairly high, for instance, with the oxygen impurity in GaP, which is in state 2, where $\beta=0.56$.[75,80]

The configuration-coordinate diagram of Fig. 2b illustrates the case of $\beta>1$, where the optical and thermal ionization energies differ considerably. This diagram is used to describe, for instance, the DX and EL2 centers, where this difference was experimentally revealed.[71,74–77] Such self-trapped states have a large potential barrier suppressing the return of free electrons to the localized state, thus giving rise to the phenomenon of persistent photoconductivity. In these conditions, there is no radiative capture into the impurity state. The various features of the adiabatic configurational potentials play an essential role in nonradiative trapping of free carriers.[75] We shall restrict ourselves to the simple model of two identical displaced parabolic curves, which was first proposed by Huang and Rhys[78] and is presently widely employed in the theory of multiphonon transitions. By this model

$$U_1(x)=\frac{M\omega^2x^2}{2} \tag{3}$$

$$U_1(x)=\frac{M\omega^2(x-x_0)^2}{2}-\varepsilon_T, \tag{4}$$

where M is the mass of the impurity, and ω is the vibrational frequency.

1.2. Multiphonon-assisted thermal emission

Consider first thermally-activated carrier emission from a deep center with no electric field present. For simplicity and definiteness, we shall consider electrons, although a considerable part of measurements were carried out on acceptors in Ge and Si. The model to be treated here is equally applicable to the electrons and holes.

Classical approximation gives the following expression for the emission probability

$$e\propto\exp-\left(\frac{\varepsilon_T+\varepsilon_2}{k_BT}\right), \tag{5}$$

where $\varepsilon_2=U_1(x_c)$, and x_c is the coordinate at the intersection of the potentials $U_1(x)$ and $U_2(x)$, at which the electron binding energy is zero, $\varepsilon_b(x_c)=0$ (see Fig. 2). Thus $\varepsilon_T+\varepsilon_2$ is actually the lowest excitation energy required to detach the electron within the classical approach to the motion of impurities. The model of Huang and Rhys, where the adiabatic potentials $U_1(x)$ and $U_2(x)$ are two identical parabolic curves, $\varepsilon_2=(\varepsilon_T-\Delta\varepsilon)^2/4\Delta\varepsilon$. In the weak-binding case ($\Delta\varepsilon\ll\varepsilon_T$), where $\varepsilon_2\gg\varepsilon_T$, no process with an activation energy $\varepsilon_T+\varepsilon_2$ was ever observed to follow relation (5). Usually the activation energy is much less than $\varepsilon_T+\varepsilon_2$, since the electron is emitted from the vibrational level lying at $\varepsilon_T+\mathscr{E}$ (the energy $\mathscr{E}$ is reckoned from the minimum of potential U_2, and $\mathscr{E}<\varepsilon_2$) because the defect tunnels from the configuration corresponding to the ground state to that of the ionized impurity (Fig. 2). As the vibrational energy $\varepsilon_T+\mathscr{E}$ increases, the tunneling barrier separating the U_1 and U_2 potentials becomes lower, and, hence, the tunneling probability increases. On the other hand, the population of the $\varepsilon_T+\mathscr{E}$ level decreases with increasing $\mathscr{E}$ proportional to $\exp(-\mathscr{E}/k_BT)$. Thus for each temperature there is an optimum energy $\mathscr{E}=\mathscr{E}_0$, at which the tunneling probability is the largest.[75,81–83]

We shall consider the defect tunneling process in semiclassical approximation. In this approach, the particle has a well defined trajectory even under the potential barrier, where the kinetic energy is negative. The probability of thermally activated emission of a defect, $P(\mathscr{E})$, with a vibrational energy $\varepsilon_T+\mathscr{E}$ at a temperature T is given by the expression

$$P(\mathscr{E})\propto\exp(-\psi) \tag{6}$$

with

$$\psi(\mathscr{E})=\frac{\varepsilon_T+\mathscr{E}}{k_BT}+2|S(\mathscr{E})|, \tag{7}$$

where $S(\mathscr{E})$ is the action multiplied by $i/\hbar$. The first term in Eq. (7) describes the population of the $\varepsilon_T+\mathscr{E}$ level, and the second, the defect tunneling from the ground to an ionized state. Since $P(\mathscr{E})$ depends exponentially on energy $\mathscr{E}$, tunneling occurs within a narrow energy interval close to the energy of optimum tunneling $\mathscr{E}_0$ (see Fig. 2). This optimum tunneling energy is determined by the vibrational energy at which $\Psi(\mathscr{E})$ has a minimum:

$$\left.\frac{d\psi}{d\mathscr{E}}\right|_{\mathscr{E}=\mathscr{E}_0}=2\left.\frac{d|S(\mathscr{E})|}{d\mathscr{E}}\right|_{\mathscr{E}=\mathscr{E}_0}+\frac{1}{k_BT}=0. \tag{8}$$

The derivative $d|S|/d\mathscr{E}$ in Eq. (8) multiplied by $\hbar$ determines the tunneling time through the barrier τ.[84,85] Thus in the case of multiphonon tunneling ionization the time of tunneling by the optimum trajectory is determined by temperature and is $\hbar/k_BT$.

Following Refs. 75, 81–83, $S(E)$ can be divided into two parts:

$$S(\mathscr{E})=-S_1(\mathscr{E})+S_2(\mathscr{E}), \tag{9}$$

$$S_i(\mathscr{E})=\frac{\sqrt{2M}}{\hbar}\int_{a_i}^{x_c}dx\sqrt{U_i(x)-\mathscr{E}},\quad i=1,2, \tag{10}$$

corresponding to two parts of the tunneling trajectory, namely, 1, under potential U_1, from the turning point a_1 to point x_c, where the adiabatic potential curves cross, and 2, under potential U_2, from a_2 to x_c. The actual direction of tunneling along the x coordinate is specified by the sign of S_i in Eq. (9). The tunneling trajectories for both adiabatic potential configurations are denoted in Fig. 2 by arrows. Tunneling in the two configurational potentials shown in Figs. 2a and 2b is essentially different in that $S_1(\mathscr{E})$ and $S_2(\mathscr{E})$ have the same sign in the case of weak electron-phonon coupling with $\beta<1$ (Fig. 2a) and opposite signs in the case of self-trapping, $\beta>1$ (Fig. 2b).[86] Recalling that $|S_2|>|S_1|$ we come to $|S_1|=|S_2|-|S_1|$ for the configuration of Fig. 2a, and to $|S|=|S_1|+|S_2|$ for the self-trapping case. Introduce the tunneling times τ_1 and τ_2 under the corresponding adiabatic potentials for the optimum energy of thermally activated tunneling:

$$\tau_i=\hbar\left.\frac{d|S_i|}{d\mathscr{E}}\right|_{\mathscr{E}=\mathscr{E}_0}=\sqrt{\frac{M}{2}}\left|\int_{a_i}^{x_c}\frac{dx}{\sqrt{U_i(x)-\mathscr{E}_0}}\right| \quad i=1,2. \tag{11}$$

Equations (8) and (11) yield

$$\tau=\tau_2\pm\tau_1=\frac{\hbar}{2k_BT} \tag{12}$$

where the minus sign corresponds to the configuration of Fig. 2a, and the plus, to that of Fig. 2b. Since $\mathscr{E}_0$ is usually much less than ε_T, the time τ_1 is practically temperature-independent and can be calculated for $\mathscr{E}_0=0$.

In the case of weak electron-phonon coupling ($\varepsilon_2\gg\varepsilon_T$), Eq. (8) yields within the Huang–Rhys model a simple relation for the optimum defect-tunneling energy $\mathscr{E}_0$

$$\mathscr{E}_0=\varepsilon_T/[\exp(\hbar\omega/k_BT)-1]. \tag{13}$$

which shows that in the low-temperature domain ($k_BT<\hbar\omega$) we indeed have $\mathscr{E}_0\ll\varepsilon_T$. Setting $\mathscr{E}_0=0$ in Eq. (11) in the calculation of τ_1 we come to

$$\tau_1=\sqrt{\frac{M}{2}}\int_{a_1}^{x_c}\frac{dx}{\sqrt{U_1(x)}} \tag{14}$$

Equation (14) yields in the case of weak electron-phonon coupling, $\beta<1$, the following expression for the tunneling time τ_1:

$$\tau_1=\frac{1}{2\omega}\ln\frac{\varepsilon_T}{\varepsilon_{\rm opt}-\varepsilon_T} \tag{15}$$

and for the self-trapping case ($\beta>1$):

$$\tau_1=\frac{1}{2\omega}\ln\frac{\varepsilon_{\rm opt}-\varepsilon_T}{\varepsilon_T}. \tag{16}$$

Thus Eq. (12) defines the temperature dependence of the tunneling time τ_2.

1.3. Multiphonon-assisted tunneling ionization in an electric field

Carrier emission in static electric fields was first considered in Ref. 87 and calculated numerically in Ref. 88; analytical expressions for the probability of deep impurity-center ionization were obtained in Refs. 89, 90, and the subsequent analysis will draw essentially from the latter works.

In a uniform electric field, the potential with a constant slope in the field-vector direction is added to the potential well binding the electron to the impurity. The electron is now capable of tunneling through the triangular potential barrier thus formed at a negative kinetic energy $-\varepsilon$ (Fig. 3), with the corresponding adiabatic potential shifted down in energy, $U_{2\varepsilon}=U_2-\varepsilon$ (dashed line in Fig. 2). In these conditions, the defect tunneling trajectory in configuration space shortens, and the barrier height becomes lower. We start by considering the case of high temperatures and relatively weak fields, where the field introduces a correction only to thermal ionization, and ε is much smaller than $\mathscr{E}_0$. The optimum defect tunneling energy $\mathscr{E}_0$ remains here unchanged, and, to first order in ε, the correction to the argument of the exponential

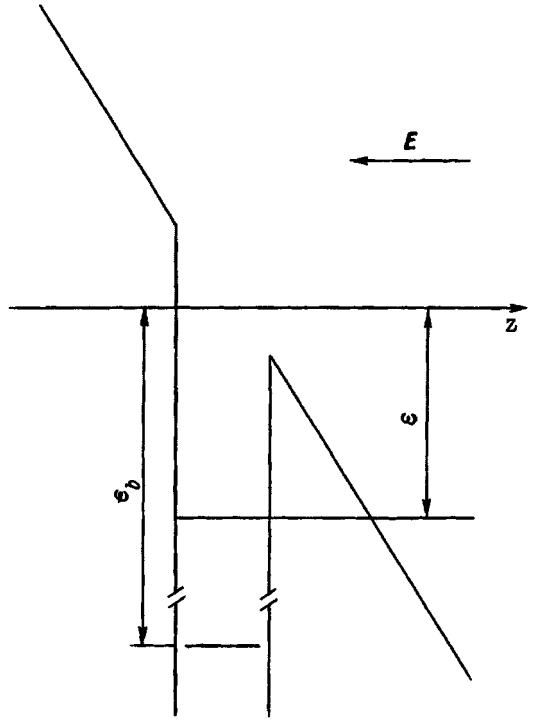

FIG. 3. Potential barrier for the electron in a dc electric field directed along the z axis. ε_b is the electron binding energy, ε is the electron escape energy.

Ψ determining the ionization probability [see Eqs. (6) and (7)] can be found by varying in ε the function $S(\mathscr{E}_0,\varepsilon)$ defined by Eqs. (9) and (10), with U_2 being replaced by $U_{2\varepsilon}$. We obtain

$$\psi(\mathscr{E}_0,\varepsilon)=\psi|_{\varepsilon=0}+2\left.\frac{d|S_{2\varepsilon}|}{d\varepsilon}\right|_{\varepsilon=0,\,x_\varepsilon=\text{const}}, \tag{17}$$

where

$$S_{2\varepsilon}=\frac{\sqrt{2M}}{\hbar}\int_{a_2}^{x_c}dx\sqrt{U_2(x)-\varepsilon-\mathscr{E}_0}. \tag{18}$$

The probability for a thermally-emitted carrier with kinetic energy $-\varepsilon$ now becomes

$$e(\varepsilon)=e(0)\exp(2\varepsilon\tau_2/\hbar) \tag{19}$$

where τ_2 is the tunneling time defined by Eq. (11), and $e(0)$ is the ionization probability with no electric field present. The increase of the probability of electron emission with energy $-\varepsilon$ by the factor $\exp(2\varepsilon\tau_2/\hbar)$ is primarily due to the lowering of barrier height when the defect is tunneling from point x_c to the turning point under the adiabatic potential curve $U_{2\varepsilon}$ at the vibrational level $\mathscr{E}_0$. While this factor grows with ε, the probability of electron tunneling through the triangular barrier whose height is determined by ε (see Fig. 3) drops rapidly proportional to $\exp[-(4\varepsilon^{2/3}\sqrt{2m^*}/(3\hbar eE)]$, where E is the electric field, and m^* is the electron effective mass. Thus the probability of multiphonon tunneling ionization with the electron escaping with a negative energy $-\varepsilon$ can be written as

$$e(E,\varepsilon)\propto\exp(2\varepsilon\tau_2/\hbar)\exp\left(-\frac{4}{3}\frac{\varepsilon^{3/2}\sqrt{2m^*}}{\hbar eE}\right). \tag{20}$$

The exponential behavior of $e(E,\varepsilon)$ results in the existence of an optimum electron energy $-\varepsilon_m$ determined by the maximum of the exponential in Eq. (20):

$$\varepsilon_m=\frac{\tau_2^2e^2E^2}{2m^*} \tag{21}$$

This optimum electron energy ε_m corresponds to the energy at which the time of electron tunneling in an electric field E is equal to the time τ_2 determining the defect tunneling under the potential curve U_2 at the vibrational level $\mathscr{E}_0$ optimum for thermally stimulated tunneling. Indeed, the tunneling time in an electric field E under a triangular barrier of height ε is given by the relation

$$\tau_e=\sqrt{\frac{m^*}{2}}\int_0^{z_f}\frac{dz}{\sqrt{(\varepsilon-eEz)}}=\frac{\sqrt{2m^*\varepsilon}}{eE}. \tag{22}$$

As follows from Eqs. (21) and (22), $\tau_e=\tau_2$ for $\varepsilon=\varepsilon_m$. Thus the result obtained has a simple physical interpretation, namely, the optimum electron energy is determined by the equality of the tunneling time of the electron in an electric field to that of the defect in configuration space under the potential U_2 corresponding to the defect without the electron.

Inserting ε_m thus found into Eq. (20) yields for the multiphonon tunneling ionization probability as a function of electric field the following expression:

$$e(E)=e(0)\exp\left(\frac{E^2}{E_c^2}\right)=e(0)\exp\left(\frac{\tau_2^3e^2E^2}{3m^*\hbar}\right). \tag{23}$$

The emission in an electric field increases by a factor $\exp(E^2/E_c^2)$, where $E_c^2=(3m^*\hbar)/(\tau_2^3e^2)$ is the characteristic field determined by the tunneling time τ_2 and, hence, depending on temperature. As seen from Eqs. (23) and (12), the ionization probability grows exponentially with squared electric field, and increases rapidly with decreasing temperature. The increase of the ratio $e(E)/e(0)$ with decreasing temperature is accounted for by the fact that at low temperatures the optimum energy $\mathscr{E}_0$ for thermally stimulated tunneling tends to zero, and the tunneling time τ_2 grows to infinity. Hence a small decrease of the adiabatic potential U_2 of an ionized impurity leads to a large increase of the emission probability. The temperature and field behavior of the carrier emission probability in a dc electric field was observed to follow Eq. (23).[90–92]

1.4. Direct ionization by electron tunneling

The emission probability as a function of electric field in Eq. (23) was obtained with due account of the fact that the corrections to multiphonon emission resulting from electron tunneling are small, in other words, that the energy of electron tunneling ε_m is much smaller than that of defect tunneling $\mathscr{E}_0$ and of thermally stimulated ionization ε_T. This condition defines the upper bound on the electric field where the consideration presented in Sec. 1.3 is valid:

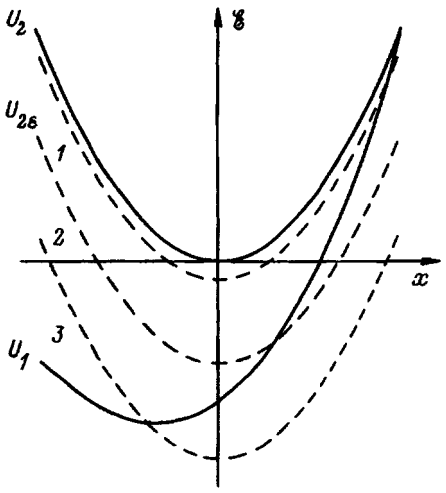

FIG. 4. Adiabatic potentials as a function of the configuration coordinate. The potential curve $U_1(x)$ relates to the case where the electron is bound to the impurity, and $U_2(x)$, to that of the ionized impurity and a free electron with zero kinetic energy. Dashed lines specify the $U_{2\varepsilon}(x)$ potentials for three characteristic cases: *1* multiphonon tunneling, *2* intermediate case, *3* direct electron tunneling.

$$E\ll E_0/2\omega\tau_2 \tag{24}$$

where

$$E_0=\frac{2\omega\sqrt{2m^*\varepsilon_T}}{e}. \tag{25}$$

In the opposite limit, $E\gg E_0$, direct carrier tunneling from the ground state to continuum, without participation of phonons, becomes dominant. The positions of the adiabatic potential curves $U_{2\varepsilon}$ for various electron kinetic energies are shown in Fig. 4. Direct electron tunneling occurs at the vibrational level at the crossing of the $U_{2\varepsilon}$ and U_1 potential curves, where an electronic transition does not involve a change in the configuration coordinate. In the low-temperature limit, where thermal excitation is not likely, direct tunneling occurs at the point where the $U_{2\varepsilon}$ curve intersects the minimum of potential U_1 at $\varepsilon=\varepsilon_{\rm opt}$. The ionization probability is determined here by electron tunneling through the triangular potential of height $\varepsilon_{\rm opt}$ (Ref. 93):

$$e(E)=\frac{eE}{2\sqrt{2m\varepsilon_{\rm opt}}}\exp(-\phi), \tag{26}$$

where

$$\varphi=\frac{4}{3}\frac{\varepsilon_{\rm opt}^{3/2}\sqrt{2m^*}}{\hbar eE}. \tag{27}$$

As the temperature increases, one will have to take into account the possibility of thermal activation of the impurity. In the case where $U_{2\varepsilon}$ crosses the U_1 parabolic curve close to its minimum, multiphonon transitions result in a correction to φ which, while being temperature-dependent, is insignificant in the strong-field domain.[90] Equations (26) and (27) show that the emission probability in direct tunneling depends on electric field weaker than under conditions of the multiphonon-assisted process (Eq. (23).

In conclusion to this Section we present a general expression obtained[90] in the frame of the Huang and Rhys model:

$$e(\mathscr{E}) \propto \exp(-\varphi), \tag{28}$$

$$\varphi = \frac{\varepsilon_T}{\hbar\omega}\,|1-y|\left[\pm 2\omega\tau_2(y) - (1+\xi^2)^{1/2} + \xi\cosh\frac{1}{2}\Theta\right] + \frac{2}{3}E_0 y^{3/2}/E, \tag{29}$$

where

$$2\omega\tau_2(y) = \frac{1}{2}\Theta \pm \ln\frac{1+(1+\xi^2)^{1/2}}{\xi^2}, \quad \Theta = \frac{\hbar\omega}{k_{\mathrm{B}}T}, \tag{30}$$

$$\xi = \left[\tilde{c}\left|1-y\right|\sinh\frac{1}{2}\Theta\right]^{-1}, \quad \tilde{c} = \frac{\varepsilon_T}{\Delta\varepsilon} = -1 + \frac{4}{b}. \tag{31}$$

The plus and minus signs in the expression for φ refer to the cases of $y<1$ and $y>1$, respectively, and the value of y is found by solving the equation

$$(E/E_0)\sqrt{y} = 2\omega\tau_2(y). \tag{32}$$

The above expressions determine the character of the exponential dependence within a broad range of electric fields and temperatures and reduces to the limiting cases described by Eqs. (23) and (26).

1.5. Charge effect

Most deep centers bear a charge, which should be taken into account when considering ionization processes. There is the well-known Poole–Frenkel effect consisting in a decrease of the thermal ionization energy of attractive Coulomb centers in the presence of an external electric field, which lowers the barrier generated by the Coulomb potential (see Fig. 5). The theory of this effect was developed by Frenkel,[94] who showed that the ionization probability grows exponentially with the square root of the external electric field. The Poole–Frenkel effect is a dominant mechanism in the increase of the ionization probability of attractive centers by electric field for not too high fields, where the ejection is dominated by over-barrier emission, and carrier tunneling does not play a significant role.[75] This phenomenon was observed in $I-V$ characteristics under a dc bias in a large number of insulators and semiconductors. Straightforward calculation shows that application of an electric field E lowers the ionization barrier in the direction opposite to the field (Fig. 5b) by an amount ε_{PF}:

$$\varepsilon_{PF} = 2\sqrt{\frac{Ze^3E}{\varkappa}}, \tag{33}$$

where Z is the charge on the center, and $\varkappa$ is the dielectric constant.

As a result, an electric field increases the probability of thermal emission

$$e(E) \propto \exp(\varepsilon_{PF}/k_{\mathrm{B}}T). \tag{34}$$

The general theory of the Poole–Frenkel effect and the deviations from the simple relations (33) and (34) are considered in detail in Ref. 83. It can be shown[75,95] that inclusion of multiphonon effects results in k_BT in Eq. (34) being replaced by $k_{\mathrm{B}}T^*$, where

$$\frac{1}{k_BT^*} = \frac{\tau_2}{\hbar} = \frac{1}{k_{\mathrm{B}}T} \pm \frac{2\tau_1}{\hbar}. \tag{35}$$

The plus sign corresponds here to the case of weak electron-phonon coupling, and the minus, to self-trapping, thus reducing or increasing, respectively, the slope of the $\ln[e(E)] \propto \sqrt{E}$ relation.

Obviously enough, the Poole–Frenkel effect can take place in relatively weak fields, where the lowering of the barrier does not exceed the Coulomb energy scale in semiconductors, i.e. in electric fields E lower than the field determined from the equation $\varepsilon_{PF}(E) = Z^2Ry^*$, where $Ry^* = e^4m^*/2\varkappa^2\hbar^2$ is the effective electron energy in the Coulomb potential of a charged impurity (the Rydberg energy). In stronger electric fields or at lower temperatures, tunneling effects become dominant, with the role of the charge being reduced to increasing the transparency of the barrier through the lowering of its height. In this limit one

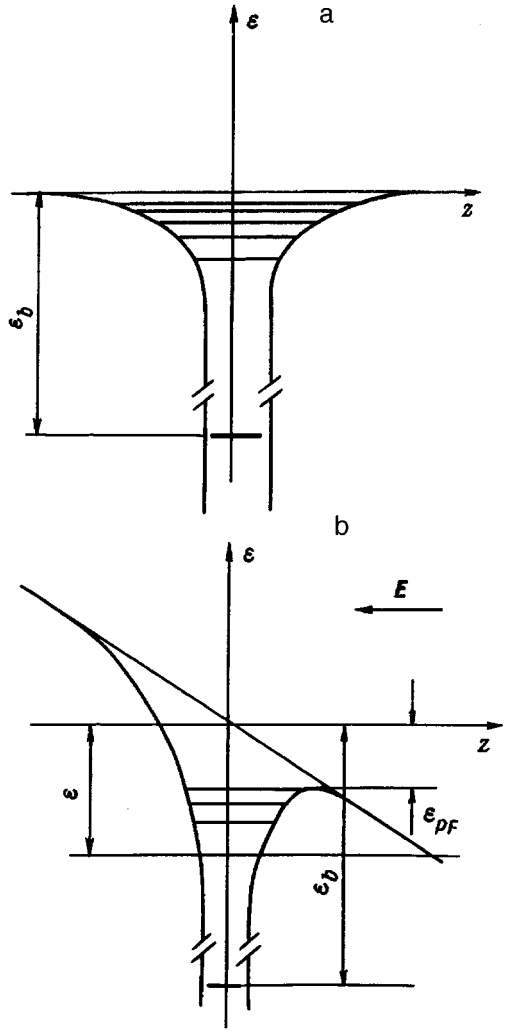

FIG. 5. Coulomb potential of an attractive impurity (a) with no electric field and (b) in the presence of a dc electric field applied along the z axis. ε_b—binding energy, ε_{PF}—lowering of the potential barrier by the Poole–Frenkel effect.

can readily obtain an expression for the correction to the probability of tunneling ionization involving a multiphonon transition. In the limit that $\varepsilon_m > Ry^*$, this correction calculated in Ref. 95 produces an additional factor in Eq. (23) for the emission probability $e(E)$. Taking into account the Coulomb charge, the probability of multiphonon-assisted tunneling ionization can be written as

$$e(E)=e(0)\exp\left[\frac{2\sqrt{2m^*Ry^*}}{eE\tau_2}\ln\left(\frac{4\tau_2{}^3e^2E^2}{m^*\hbar}\right)\right]\exp\left(\frac{\tau_2^3e^2E^2}{3m^*\hbar}\right). \tag{36}$$

We readily see that the correction due to the impurity charge in Eq. (36) tends to unity with increasing electric field and becomes insignificant in strong fields.

Thus taking into account the Poole–Frenkel effect and multiphonon tunneling ionization we come to the conclusion that the log ionization probability grows with the field first as $\sqrt{E}$ and, in the high-field domain, as E^2.

1.6. Ionization by submillimeter radiation

The choice between the quantummechanical and classical treatment of an electromagnetic field depends on the relation between the period of the radiation field Ω^{-1} and the characteristic times of the processes occurring in the system under study. Keldysh[96] showed that multiphonon ionization of semiconductors under high-frequency illumination and tunneling ionization in a dc electric field are just two limiting cases of the same nonlinear process. It was also demonstrated that, for a given incident intensity, the ionization probability increases with frequency, and that this growth is characterized by a parameter $\Omega\tau_e$, where τ_e is the electron under-barrier tunneling time in the electric wave field, with the barrier height determined by the ground-state binding energy. These results (see also Ref. 97) are fully applicable to analyzing direct electron tunneling ionization from deep centers. For these conditions, the height of the barrier for electron tunneling is determined by the electron binding energy with the impurity at equilibrium, i.e. by $\varepsilon_{\rm opt}$. The time required for an electron to tunnel through a barrier of height $\varepsilon_{\rm opt}$ in an electric field E can be written

$$\tau=\frac{\sqrt{2m^*\varepsilon_{\rm opt}}}{eE}. \tag{37}$$

If for the value of E corresponding to the maximum wave field amplitude this time is shorter than the wave period Ω^{-1}, i.e.

$$\Omega<\frac{eE}{\sqrt{2m^*\varepsilon_{\rm opt}}}, \tag{38}$$

then the action of the high-frequency field is equivalent to application of a dc electric field. The tunneling ionization probability does not depend in this case on frequency, and the tunneling probability is given by Eqs. (26) and (27). As follows from Ref. 96, where a general expression for the electron transition probability was obtained for the total frequency range, one can readily derive the frequency correction to the exponential factor in Eq. (26) if condition (38) is met:

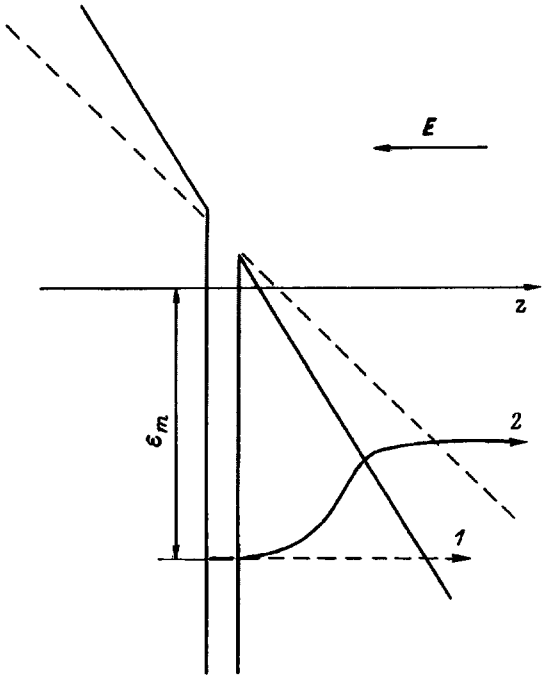

FIG. 6. Electron tunneling trajectory under a triangular barrier for an initial energy $-\varepsilon_m$ (*1*) in a dc electric field and (*2*) in an ac field. During the tunneling, the ac electric field $E\cos(\Omega t)$ changes the slope of the barrier, and the electron absorbs photons.

$$\varphi=\frac{4}{3}\frac{\sqrt{2m^*}\varepsilon_{\rm opt}^{3/2}}{\hbar eE}\left(1-\frac{m^*\Omega^2\varepsilon_{\rm opt}}{5e^2E^2}\right). \tag{39}$$

The effect of a high-frequency electric field on the ejection probability is due to two mechanisms, namely, (i) barrier modulation, and (ii) a possibility of tunneling at a lower barrier height through absorption of photons. While the first mechanism brings about an exponential decrease of the tunneling probability, the second results in its exponential growth. As the frequency is increased, the energy absorbed in tunneling increases too and tends to the binding energy, thus resulting in ionization through multiphonon absorption. The ejection probability also grows in this case with increasing frequency, since the photon energy increases, and, accordingly, the number of photon required to initiate an optical transition decreases (see Fig. 6).

While in the case of multiphonon-assisted tunneling ionization the electric field does not act on the motion of the defect itself, the tunneling of an electron should certainly change in an ac electric field. In the limit of multiphonon tunneling ionization in a dc electric field (see Sec. 1.3) we found that the optimum energy for electron tunneling ε_m is determined by the condition of the tunneling time of the electron τ_e, (22), being equal to that of the defect τ_2, with the latter being determined by the temperature and defect vibrational frequency (12):

$$\tau_e\equiv\tau_e(\varepsilon_m)=\tau_2. \tag{40}$$

The same condition determines the optimum electron energy before tunneling in an ac electric field $\varepsilon_{\rm init}=-\varepsilon_m$ (see

Fig. 6) (note that in an ac field the initial and final tunneling energies are different, because energy can be absorbed during the tunneling).

The process of multiphonon tunneling ionization can be divided into three stages: (1) thermal excitation transfers the defect with a bound electron to the vibrational level corresponding to the vibrational energy $\varepsilon_T+\mathscr{E}_0$; (2) The vibrational system undergoes rearrangement to the potential corresponding to a free electron with a negative kinetic energy $-\varepsilon_m$, i.e. the system transfers to the adiabatic potential $U_{2\varepsilon_m}$; (3) the electron tunnels to the free state with the initial energy $-\varepsilon_m$. The two latter processes are tunneling assisted. Condition (40) for determining the energy ε_m can be derived similarly to the way this was done in Sec. 1.3, if one represents the probability of electron tunneling with an initial energy $-\varepsilon$ in a general case by

$$p_e(\varepsilon)\propto\exp(-2S_e(\varepsilon)), \tag{41}$$

where $S_e(\varepsilon)$ is the electron action multiplied by $i/\hbar$, and introduces the electron tunneling time $\tau_e(\varepsilon)$ in the form

$$\tau_e(\varepsilon)=\hbar\frac{dS_e(\varepsilon)}{d\varepsilon}. \tag{42}$$

Let us calculate now ε_m as a function of frequency and wave-field amplitude under the condition that the electron tunneling time τ_e is determined by the time τ_2, and find the electron tunneling probability for these conditions. In the case of tunneling under a time-varying potential we can express S_e through the Lagrangian L_e (Ref. 98)

$$\hbar S_e(\varepsilon_m)=-\int_{-\tau_e}^{0}L_e(\tau)d\tau+\varepsilon_m\tau_e. \tag{43}$$

The dependence of the Lagrangian L_e on τ is determined by the dependence of the electron on coordinate z (Fig. 6) and velocity $\dot{z}=dz/d\tau$ at time τ:

$$L_e(\tau)=-\frac{m^*}{2}\dot{z}^2-U_e(z), \tag{44}$$

where U_e is the potential energy in an electric field. All the quantities are calculated by the rules of classical mechanics, but with due account of the fact that the time t is replaced by imaginary time $\tau=it$, since the motion takes place in the classically forbidden region under the barrier. Accordingly, in the case where the electric field vector is directed opposite to the z axis we have

$$U_e=-eEz\cos(\Omega t)=-eEz\cosh(\Omega\tau). \tag{45}$$

The tunneling trajectory $z(\tau)$ and ''velocity'' $\dot{z}(\tau)$ should be found from the classical equation of motion:

$$-m^*\frac{d^2z}{d\tau^2}=-\frac{\partial U_{2\varepsilon}}{\partial z} \tag{46}$$

subject to the boundary conditions

$$z(\tau)\big|_{\tau=\tau_e}=0 \tag{47}$$

for the tunneling beginning at the imaginary time $-\tau_e$ and

$$\dot{z}(\tau)\big|_{\tau=0}=0 \tag{48}$$

after the completion of the tunneling ($\tau=0$) at the turning point (see Fig. 6).

The minus sign of the second derivative in Eq. (46) appears as a result of the replacement of t by $i\tau$. Equation (46) reduces to the form

$$\frac{d^2z}{d\tau^2}=-\frac{eE}{m^*}\cosh\Omega\tau. \tag{49}$$

Taking into account Eqs. (47) and (48), Eq. (49) yields

$$\dot{z}=\frac{eE}{m^*\Omega}\sinh(\Omega\tau) \tag{50}$$

and

$$z=\frac{eE}{m^*\Omega^2}(\cosh(\Omega\tau_e)-\cosh(\Omega\tau)). \tag{51}$$

At the initial instant of time, $\tau=-\tau_e$, the ''velocity'' is determined by the total electron energy $-\varepsilon_m$, because the potential energy $U_e(z=0)=0$ [see Eq. (45) and Fig. 6)]. Thus we come to the condition

$$\dot{z}^2\big|_{\tau=-\tau_e}=\frac{2\varepsilon_m}{m^*} \tag{52}$$

whence follows the relation connecting ε_m with the tunneling time τ_e:

$$\varepsilon_m=\frac{(eE)^2}{2m^*\Omega^2}\sinh^2(\Omega\tau_e). \tag{53}$$

We see that for a given tunneling time τ_e the energy ε_m increases with frequency. In the limiting case of low frequencies, $\Omega\tau_e<1$, the relation between ε_m and τ_e determined by Eq. (53) coincides with Eq. (22). Note that using Eq. (43) one can readily verify that relation (42) for τ_e does indeed hold.

Equations (41), (43), (44), and (50) and (51) can be used to obtain the following relation for the electron tunneling probability $p_e(E,\Omega)$ for a fixed tunneling time τ_e:

$$p_e(E)\propto\exp\left\{-\frac{(eE)^2}{2m^*\Omega^3}\left[2\Omega\tau_e\sinh^2(\Omega\tau_e)+\Omega\tau_e-\frac{1}{2}\sinh(2\Omega\tau_e)\right]\right\}. \tag{54}$$

Taking into account Eq. (53), relation (54) agrees with exponential accuracy the result obtained in Ref. 96 and coincides with the ionization probability in an ac electric field calculated[84] in quasi-classical approximation with the use of the vector gauge, where the scalar potential is zero.

Setting $\tau_e=\tau_2$ and taking into account the increase of the defect tunneling probability under multiphonon thermally-activated ionization, which is determined by the factor $\exp(2\varepsilon_m\tau_2/\hbar)$ [see Eqs. (19) and (20) in Sec. 1.3], we obtain for the resultant probability of multiphonon-assisted defect tunneling ionization under illumination an expression similar to Eq. (23), where one should now substitute τ_2^* for τ_2:

$$e(E,\Omega)=e(0)\exp\left(\frac{\tau_2^{*3}e^2E^2}{3m^*\hbar}\right), \tag{55}$$

where

$$\tau_2^{*3}=\frac{3}{4\Omega^3}(\sinh(2\Omega\tau_2)-2\Omega\tau_2). \tag{56}$$

In the limit $\Omega\tau_2<1$ we obtain from Eq. (56):

$$\tau_2^{*3}=\tau_2^3\left[1+\frac{1}{5}(\Omega\tau_2)^2\right]. \tag{57}$$

We see that an increase in frequency results in a growth of the tunneling ionization probability, which is due to the increasing initial energy of the tunneling electron ε_m [see Eq. (53)], i.e. to the increase in absolute magnitude of the optimum electron transition energy.

The dependence of the multiphonon emission probability on electric field amplitude [both for dc, Eq. (23), and high-frequency, Eq. (55), fields] was derived under the condition that electron tunneling gives only a small correction to multiphonon-assisted emission, in other words, that the energy of electron tunneling ε_m is much less than that of defect tunneling $\mathscr{E}_0$ and thermal ionization energy ε_T. This condition determines the upper limit to the electric fields for which the above consideration is valid.

2. EXPERIMENTAL METHODS AND SUBJECTS OF INVESTIGATION

Ionization of deep impurities by high-intensity submillimeter radiation was discovered and studied in a large number of semiconductors containing such impurities. One measured the photoresponse of a sample to pulsed radiation of a submillimeter laser, which is generated by a change in free carrier concentration through impurity ionization. The radiation sources used were TEA CO_2-pumped, high-power tunable submillimeter pulsed molecular-gas lasers with NH_3, CH_3F, and D_2O. The principle of operation of such lasers was developed and used to achieve cw lasing by Chang and Bridges in 1969[1] and, in 1974, de Temple extended it to obtain pulsed laser operation.[2] The choice of the CO_2 laser for optical pumping was based on the ability of tuning it within the 9.2–10.6 μm-range, which includes strong vibrational-rotational absorption lines of many molecules. More than 1000 compounds are presently employed as gain media for CO_2-pumped lasers.[99] The use for pumping of high-intensity radiation from TEA CO_2 lasers operating at 100 kW and more opens new possibilities in this respect, since the strong electric field of the light wave results in a broadening of molecular levels and permits one to excite states fairly distant from the pumping frequency.[2] One can thus achieve lasing at a number of wavelengths which would not be accessible with low-power cw-pump radiation. The search for conditions favorable for lasing in the FIR-SBM range reduces primarily to finding appropriate gain media and lines for the CO_2 pumping laser which would be in resonance with the corresponding molecular transitions. Thousands of lines covering the whole range of FIR-SBM radiation (20 μm to 2 mm) have thus far been found for most of the media.[99–104] Looking for new lasing lines is, however, not as essential for semiconductor research as finding strong and stable, single radiation lines. This is particularly important for pulsed lasers, whose high-power pump radiation results in broadening of the gain-medium molecular levels and, hence, in observation of a large number of additional lines.

TABLE I. Characteristics of the strong individual lasing lines used in this work.

Wavelength μm	Line of CO_2 pump-laser	Maximum intensity, kW/cm^2	Medium
35	10P (24)	300	NH_3
66	9P (32)	100	D_2O
76	10P (26)	4000	NH_3
90.5	9R (16)	5000	NH_3
148	9P (36)	4500	NH_3
152	10P (32)	3000	NH_3
250	9R (26)	400	CH_3F
256	10R (14)	500	NH_3
280	10R (8)	1000	NH_3
385	9R (22)	5	D_2O
496	9R (20)	10	CH_3F

The most sophisticated element in the laser system under consideration is the pumping laser. In earlier days, development of an optically pumped laser required, in the first place, building in the laboratory a high-power pulsed CO_2 laser with a high level of suppression of electromagnetic interference, which was an obstacle to extending the range of applicability of high-excitation FIR-SBM spectroscopy. Now the availability of high-stability, high-power commercial TEA CO_2 lasers (URANIT 104, 204) permits one to assemble such a system with no difficulties at all. The characteristics of strong single lines covering the range from 30 to 500 μm, the corresponding gain media and lines of the TEA CO_2 laser which are used for pumping are listed in Table I. The photon energies corresponding to these wavelengths lie in the 35–2 meV range and in all cases are substantially lower than the binding energies of the deep impurities studied. The radiation pulse length varied for different lines from 10 to 100 ns. The radiated power was $\sim$50 kW. The radiation was focused to a spot of about 1 mm^2, with the maximum intensity reaching as high as 5 MW/cm^2. More details on the system can be found in Refs. 11, 48.

The intensity, shape and spatial distribution of the laser radiations were monitored with fast noncooled photodetectors operating in the submillimeter range and based on the photon drag effect,[63] intraband μ-photoconductivity,[64] stimulated tunneling effect in metal/semiconductor structures under plasma reflection,[58,66] as well as with the Spirikon pyroelectric array. The pulsed signal proportional to the change in sample resistance under laser illumination was measured in a standard photoresponse measurement circuit with a load resistance $R_L=50\ \Omega$ (see inset to Fig. 7). The bias voltage across the sample, 5 V/cm, was substantially lower than the impurity avalanche-breakdown threshold. The measurements were carried out within the 30–150 K range, where at thermal equilibrium practically all carriers are frozen out on the impurity. The samples were placed in an optical cryostat. Penetration of light in the medium IR range into the cryostat was prevented by the use of crystalline quartz filters and, in the visible, by a 1-mm thick black-polyethylene filter.

The tunneling ionization processes were studied on deep

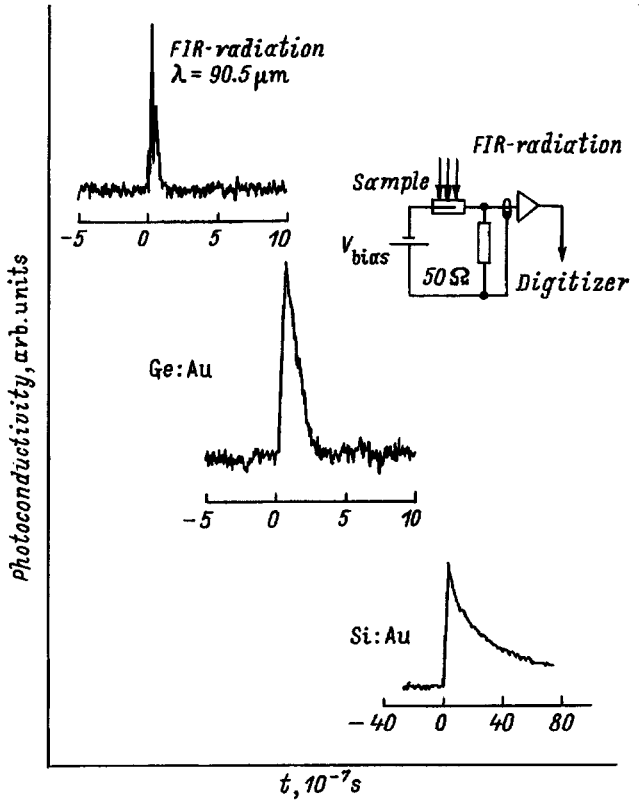

FIG. 7. Oscillographic traces of the excitation pulse and of the photoconductive signals generated in a sample with deep impurities illuminated by FIR–SBM radiation. Inset shows the measurement circuit.

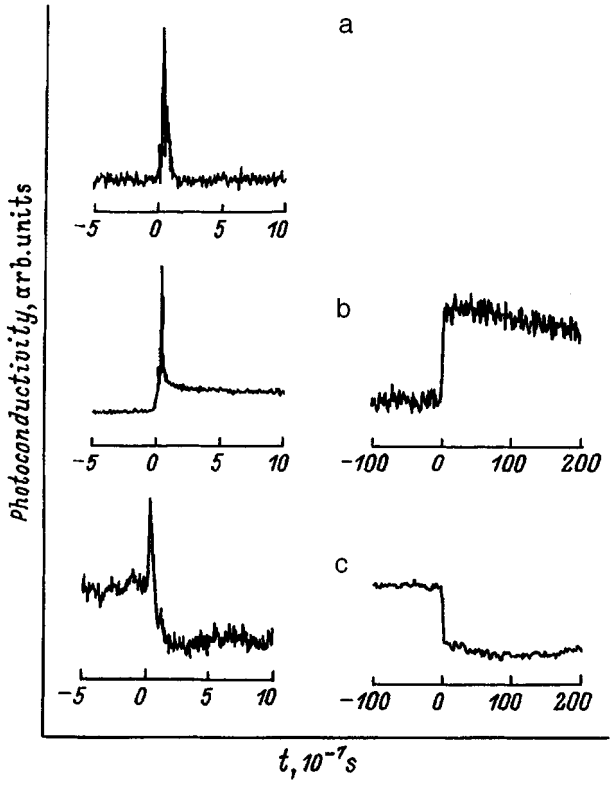

FIG. 8. Oscillographic traces of (a) excitation pulse with $\lambda = 90.5$ μm and of the photoconductive signals generated by illuminating with FIR-SBM radiation an $Al_{0.5}Ga_{0.5}Sb$ sample (b) in the dark and (c) in the state of persistent photoconductivity produced by exposing the sample preliminarily to light in the near IR range.

impurity centers of two different types, namely, (i) those with weak electron-phonon coupling, $\beta < 1$ (Au, Hg, Cu, Zn in germanium, Au in silicon, and Te in gallium phosphide) and (ii) with strong electron-phonon coupling where self-trapping takes place, $\beta > 1$ (tellurium in $Al_xGa_{1-x}Sb$ and $Al_xGa_{1-x}As$).

The thermal ionization energy of acceptor impurities ε_T in germanium was 150 meV (Au), 90 meV (Hg), 40 meV (Cu), and 30 meV (Zn), for Au in silicon—300 meV, and for the donor tellurium in gallium phosphide, 90 meV (Ref. 75). Note that tellurium in gallium phosphide is essentially a deeply-buried shallow Coulomb center.

Doping with tellurium of $Al_xGa_{1-x}Sb$ samples with $x = 0.28$ and 0.5, and of $Al_xGa_{1-x}As$ with $x = 0.35$ resulted in electronic conduction, and one observed all the main features characteristic of DX centers, in particular, the persistent photoconductivity.[105,106]

3. OBSERVATION OF THE TUNNELING IONIZATION OF DEEP-IMPURITY CENTERS BY HIGH-INTENSITY FIR-SBM RADIATION

Semiconductors containing deep and shallow impurity centers have been used successfully already for a long time as low-temperature detectors in the IR and FIR ranges.[107] The long-wavelength limit to their use is bounded by the binding energy of the impurity, with no response obtained from deep centers such as, for instance, Ge:Au and Ge:Hg in the FIR and, all the more so, in the submillimeter regions of the spectrum. This pattern is observed, however, only at relatively low light intensities. Excitation of a semiconductor containing generated deep impurities by strong pulsed FIR-SBM laser radiation produced a photoconductive signal by ionizing the deep impurity centers, despite the fact that the pump photon energy was tens of times lower than their thermal ionization energy, ε_T.[69,108–111] A signal which increased superlinearly with the incident intensity was observed from all studied samples of Ge, Si, GaP, $Al_xGa_{1-x}As$, and $Al_xGa_{1-x}Sb$ within a broad range of temperatures and wavelengths employed.[86] The sign of the photoconductive signal corresponds to a decrease of the sample resistance, and its characteristic decay time is different for different types of impurities and different temperatures. The length of the photoresponse pulse for deep substitutional impurities is somewhat longer than that of the laser pulse (Fig. 7) and varies depending on temperature from 100 ns to 10 μs, which corresponds to the photoexcited carrier lifetimes (see, e.g., Refs. 75, 112, 113). In the case of self-trapped DX^- centers in $Al_xGa_{1-x}Sb$ and $Al_xGa_{1-x}As$ one observes an increase in sample conductivity which persists for several hundreds of seconds after the excitation pulse, which is characteristic of the decay of persistent photoconductivity in the samples with DX^- centers. Figure 8 compares photoresponse signals obtained from an $Al_xGa_{1-x}Sb$ sample on two time scales (Fig. 8b) with the pump pulse (Fig 8a). The observation of positive persistent photoconductivity under FIR-SBM excitation suggests that this signal is due to electron detachment from the DX centers.

Variation of the sample conductivity induced by SBM radiation can be due either to processes involving radiation absorption by free carriers (electron gas heating, μ photoconductivity) or to the appearance of additional free carriers in ionization.

We shall dwell first on the possible effect of heating the lattice or the electron gas, since this is the most natural mechanism of photoconductivity under intense illumination. Carrier heating was studied in detail in the submillimeter range samples with shallow impurities and at not too low temperatures, i.e. where the impurities are ionized and the conditions are most favorable for heating. As follows from these studies, presented in the Appendix, in the case of excitation of samples with deep impurities, electron gas heating can be excluded as the cause of the observed impurity ionization based on the kinetics of the detected signals. To begin with, electron gas heating in the temperature and concentration ranges considered here should produce negative photoconduction, whereas the photoconductivity observed experimentally is positive. Besides, the photoresponse signal due to electron heating should either reproduce in shape the pump pulse or be more complex, but it should not be longer than the latter (see Appendix and Refs. 39, 114), whereas the observed signals correspond to excited-carrier trapping times and are substantially longer than the pump pulses. The impurity ionization manifests itself most clearly in the case of submillimeter-range persistent photoconductivity in samples containing DX centers.

Thus observation of positive photoconductive signals with times substantially in excess of the pump pulse length excludes electron gas heating and the corresponding photoconductivity as a possible mechanism of the observed photoresponse (see Appendix). The suppression of heating in samples doped primarily by deep centers and maintained at sufficiently low temperatures is due to carrier freezeout at impurities and, hence, to the absence of noticeable radiation absorption. Thus the photoresponse is indeed caused by photoionization of deep impurities by light with the photon energy $\hbar\Omega$ much less than the thermal ionization energy of impurities ε_T.

Figure 9 displays the dependence of the photoresponse of mercury-doped germanium samples ($\varepsilon_T=90$ meV) on light intensity measured at $T=64$ K for two different wavelengths. Shown in Fig. 10 on a semilog scale are similar data obtained for another deep impurity (gold in germanium) for three wavelengths. The quantities σ_i and σ_d are the sample conductivities under illumination and in the dark, respectively. Since the pump pulse duration is shorter than the nonequilibrium-carrier trapping time, recombination during the excitation can be disregarded. Therefore the experimentally determined relative change in conductivity, $\Delta\sigma/\sigma_d=(\sigma_i-\sigma_d)/\sigma_d$, corresponds to the relative change in the free-carrier concentration, which, in its turn, is proportional to the change in the impurity ionization probability.

Deep-impurity photoionization by light with $\hbar\Omega<\varepsilon_T$ and the strong nonlinear dependence of this process on pump intensity can be related to several mechanisms of nonequilibrium carrier generation, such as multiphoton-assisted ionization,[13] tunneling ionization involving photon

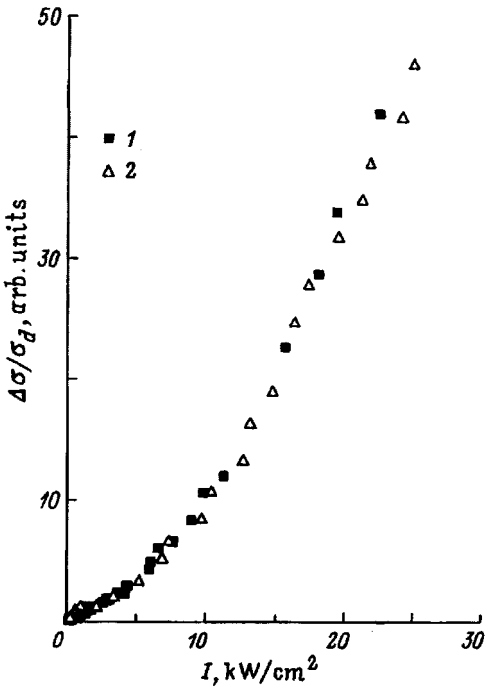

FIG. 9. Relative change in conductivity, $\Delta\sigma/\sigma_d=(\sigma_i-\sigma_d)/\sigma_d$, of Hg-doped germanium samples ($\varepsilon_T=90$ meV) measured at $T=64$ K vs light intensity for various wavelengths $\lambda(\mu\text{m})$: (*1*) 90.5 and (*2*) 250.

absorption,[18] light-induced impact ionization,[33,34,115] and multiphonon-assisted or direct tunneling in the electric wave field.[69,108] These processes depend differently on the radiation frequency. An increase in radiation frequency boosts the rate of nonequilibrium carrier generation through multiphonon absorption and tunneling ionization involving pho-

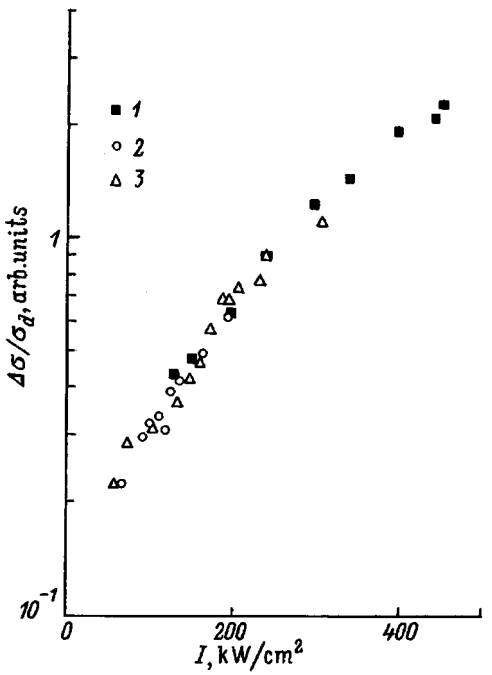

FIG. 10. Relative change in conductivity, $\Delta\sigma/\sigma_d=(\sigma_i-\sigma_d)/\sigma_d$, of Au-doped germanium samples ($\varepsilon_T=150$ meV) measured at $T=77$ K *vs* light intensity for various wavelengths $\lambda(\mu\text{m})$: (*1*) 90.5, (*2*) 152, and (*3*) 250. The plots are on a semilog scale.

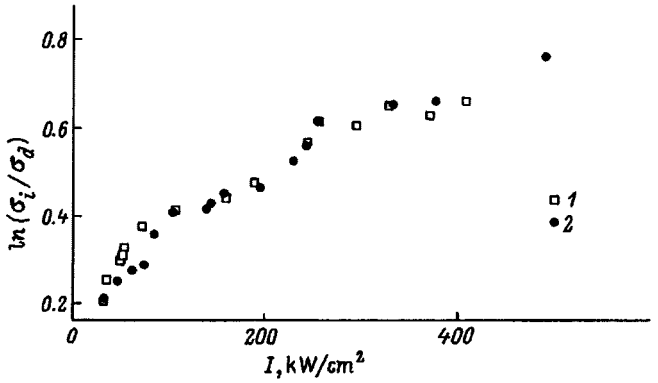

FIG. 11. Log conductivity ratio under illumination and in the dark, $\ln(\sigma_i/\sigma_d)$, of Au-doped germanium samples ($\varepsilon_T=150$ meV) measured at $T=77$ K *vs* intensity of (*1*) linearly and (*2*) circularly polarized pump light, $\lambda=90.5$ μm.

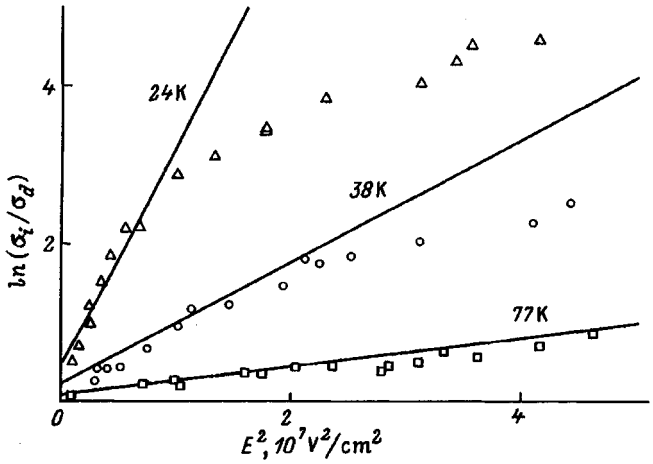

FIG. 12. Log conductivity ratio under illumination and in the dark, $\ln(\sigma_i/\sigma_d)$, of Au-doped germanium samples ($\varepsilon_T=150$ meV) vs squared electric field amplitude of $\lambda=90.5$ μm radiation. The corresponding temperatures are specified at the curves. The straight lines are plots of the relation $e(E)\propto A\exp(E^2/E_c^2)$ constructed with E_c^2 as a fitting parameter.

ton absorption, and reduces the probability of light-induced impact ionization.[34] By contrast, tunneling ionization occurring in the field of an optical wave does not depend on frequency.

Measurements showed that at temperatures of about 70 K photoconductivity does not depend on radiation wavelength above 90 μm throughout the intensity range covered. This is demonstrated by Figs. 9 and 10, which show that the curves for all wavelengths coincide within the measurement accuracy. The signal is also independent of the radiation polarization, which is evident from Fig. 11, where the photoresponse signal in Ge:Au is presented as a function of intensity for linearly and circularly polarized light with a wavelength $\lambda=90.5$ μm. The observed independence of the signal of radiation frequency (Figs. 9 and 10) permits a conclusion that the free-carrier generation is due here to the tunneling processes,[69] with the FIR–SBM radiation acting as a dc field. The ionization probability is determined in this case by the electric field of the radiation rather than by the magnitude and number of the photons. It is in these conditions that most experiments were made whose results are discussed in detail and compared with the theory for a dc field in Sec. 4. An increase in frequency or decrease in temperature result in the onset of a frequency dependence of the ionization probability, which corresponds to increasing tunneling probability. The corresponding experimental results and the mechanisms responsible for the appearance of this frequency dependence are treated in Sec. 4.5.

4. IONIZATION OF DEEP-IMPURITY CENTERS BY HIGH-INTENSITY FIR-SBM RADIATION

4.1. Multiphonon-assisted tunneling ionization

The multiphonon tunneling ionization is characterized by an exponential dependence on the squared electric wave-field amplitude: $e(E)=e(0)\exp(E^2/E_c^2)$ (see 1.3). Such an increase in the photoconductive signal was observed for all samples within a broad range of fields and temperatures. The experimental dependences of $\ln(\sigma_i/\sigma_d)$ on squared amplitudes of the electric wave field are shown in Fig. 12 for Ge:Au and in Fig. 13 for $Al_xGa_{1-x}Sb$. The measurements were performed at different temperatures and wavelengths. We see that there exists a field interval for each temperature within which the probability of photoionization depends on electric field amplitude as $\exp(E^2/E_c^2)$. A comparison of experimental data on FIR ionization of the Au impurity in Si at $T=300$ K with earlier studies of the dependence of thermal ionization probability on dc electric field, $e(E)$, made by capacitive spectroscopy[91,92] showed that $e(E)\propto\exp(E^2/E_c^2)$ in both cases, with the values of E_c differing by a factor 1.5–2 (Fig. 14). This may be considered a good agreement between the results obtained by such different methods, if we take into account the field inhomogeneities present in a sample studied by DLTS.

Figures 12–14 also show with solid-lines plots the $A\exp(E^2/E_c^2)$ relation calculated with the fitting parameter E_c^2. As follows from Eqs. (23) and (36), the slope of the experimental curves in the field region where $\ln(\sigma_i/\sigma_d)\propto\exp(E^2/E_c^2)$ permits one to determine the tunneling times τ_2. In order to extract τ_2 from experimental data, one has to know the effective carrier mass, which determines the tunneling process. In Fig. 15, the tunneling time τ_2 is shown as

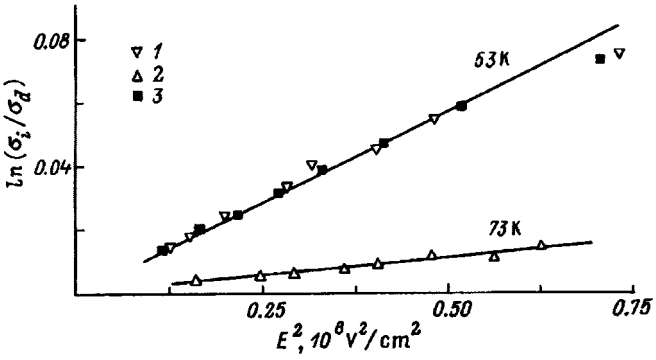

FIG. 13. Log conductivity ratio under illumination and in the dark, $\ln(\sigma_i/\sigma_d)$, of $Al_{0.5}Ga_{0.5}Sb$ samples *vs* squared electric field amplitude of the radiation. The corresponding temperatures are specified at the curves. Excitation wavelength λ(μm): (*1,2*) 90.5 and (*3*) 250. The straight lines are plots of the relation $e(E)\propto A\exp(E^2/E_c^2)$ constructed with E_c^2 as a fitting parameter.

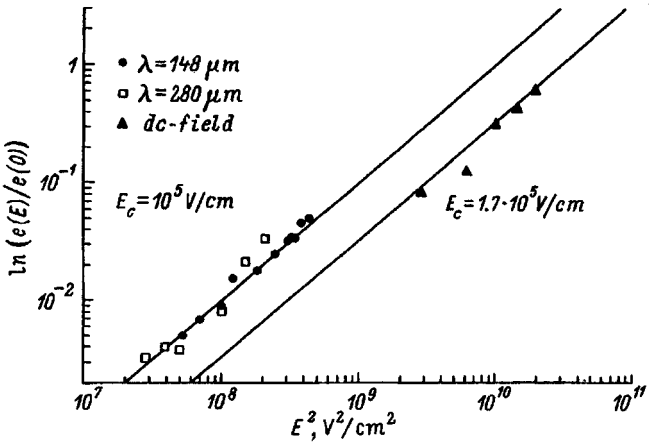

FIG. 14. Log-log plot of the probability ratio for ionization with electric field present to thermal ionization, $\ln[e(E)/e(0)]$, of the gold acceptor impurity in silicon, Si:Au, measured at $T=300$ K vs squared electric field amplitude. The data derived from the photoresponse to FIR–SBM illumination are compared with ionization measurements made in a dc electric field.[91] The straight lines are plots of the relation $e(E)\propto A\exp(E^2/E_c^2)$ constructed with E_c^2 as a fitting parameter.

a function of reciprocal temperature for a number of deep impurities studied. In the case of deep acceptors in germanium, the light-hole mass was used. Figure 15 demonstrates the good agreement of the experimental values of τ_2 with Eq. (12). One may thus conclude that carriers bound to a deep acceptor tunnel into the light-mass subband.[69] This is due to the fact that the symmetry of substitutional impurities corresponds to the point group T_d, and that the ground state of a deep impurity represents a superposition of the light- and heavy-hole states. Thus an acceptor-bound hole can be associated with neither the light nor the heavy mass. It was shown theoretically[116] that tunneling depends essentially on the wave-function tail distant from the center, and that it is the light holes that provide a major contribution to this tail.

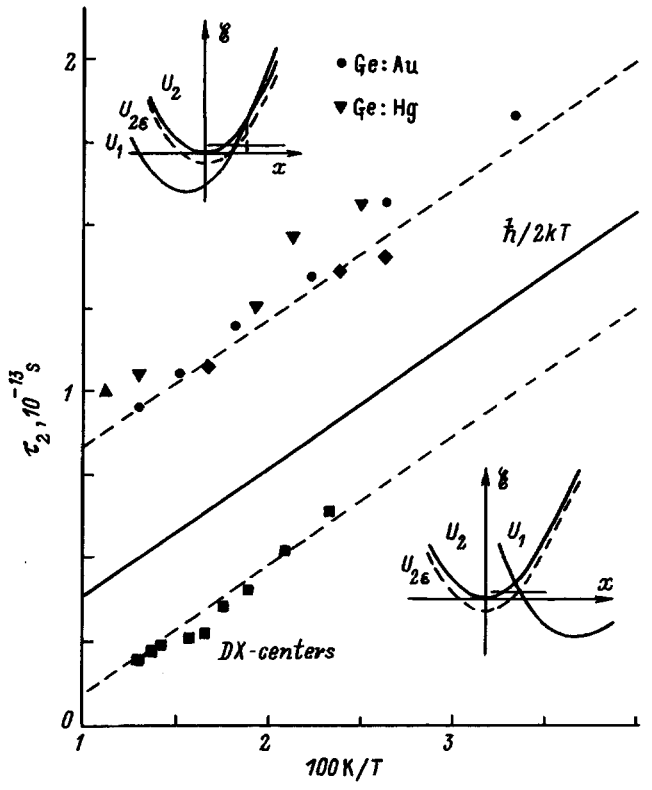

FIG. 15. Tunneling time τ_2 extracted from experimental values of E_c^2 *vs* reciprocal temperature for Au and Ge in germanium and DX centers in $Al_{0.5}Ga_{0.5}Sb$. The straight line is a plot of $\tau_2=\hbar/2k_BT$, and the dashed lines, those of $\tau_2=\hbar/2k_BT+\tau_1$ with $\tau_1=4.5\times10^{-14}$ s, and $\tau_2=\hbar/2k_BT-\tau_1$ with $\tau_1=2.9\times10^{-14}$ s. The insets shows schematically the configurational potentials corresponding to the two impurities.

For comparison, Fig. 15 shows also a plot of $\hbar/2k_BT$. We see that τ_2 is of the order of $\hbar/2k_BT$. Note, however, an essential point. As evident from the experimental data presented in Fig. 15, for any temperature τ_2 is larger than $\hbar/2k_BT$ for substitutional impurities, but less than $\hbar/2k_BBT$ for self-trapped DX^- centers. This result is in excellent agreement with theory [see Eq. (12) in Sec. 1.1)]. Thus, by determining the tunneling time from data on multiphonon tunneling ionization in a high-frequency electric field, one can unambiguously identify the type of the deep-impurity adiabatic potential.[110] The temperature-independent tunneling times $\tau_1=\tau_2-\hbar/2k_BT$ are given in the caption to Fig. 15 for different impurities.

We note in conclusion that the existence of persistent photoconductivity in $Al_xGa_{1-x}Sb$ samples permitted one to observe, besides the multiphonon tunneling ionization of DX centers, stimulated carrier trapping by the center. In this case preliminary illumination of the sample in the visible region at low temperatures ($T<100$ K) results in electron detachment from DX centers and, respectively, in an increase of the sample conductivity. Due to the persistent photoconductivity, this state persists for a long time. Subsequent illumination of the sample with FIR pulses produces a negative photoresponse signal (Sec. 2, Fig. 8b) caused by the multiphonon-stimulated carrier capture by the center in the high-frequency radiation field. This provides an additional argument for the ionization being due to multiphonon-assisted tunneling transitions.

4.2. Direct tunneling ionization

In strong electric fields, one observes transition to direct tunneling that does not involve phonons.[108] As evident from Fig. 12, photoconductive signals in strong fields are less than expected in the case of multiphonon tunneling ionization. This is seen also from Figs. 16–18, where $\ln(\sigma_i/\sigma_d)$ is plotted as a function of squared electric field E for Ge:Au and Ge:Hg for different wavelengths and temperatures. For fields in excess of E_0 the ionization probability grows slower with increasing E than that in the multiphonon tunneling region.

As shown in Sec. 1, multiphonon tunneling in an electric field gives only a correction to multiphonon-assisted thermal emission. The emission probability proportional to $\exp(E^2/E_c^2)$ was obtained taking into account the fact that the electron tunneling energy ε_m (21) is less than the optimum defect-tunneling energy $\mathscr{E}_0$ (13). The electron tunneling energy grows with electric field, thus reducing $\mathscr{E}_0$. The multiphonon tunneling approximation becomes invalid when ε_m becomes equal to $\mathscr{E}_0$. The critical value of the electric field

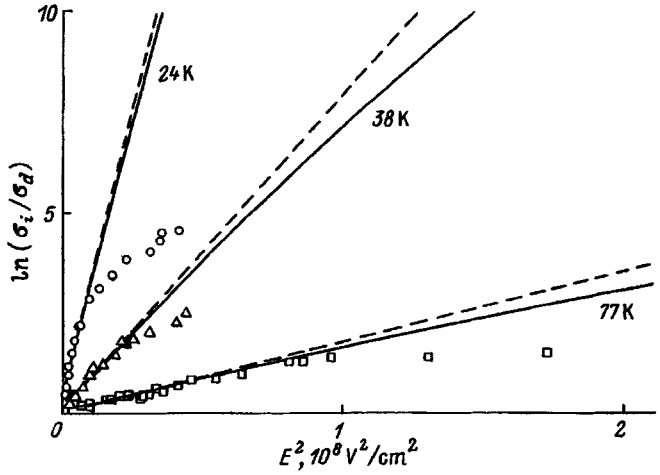

FIG. 16. Log conductivity ratio under illumination and in the dark, $\ln(\sigma_i/\sigma_d)$, of Au-doped germanium samples ($\varepsilon_T = 150$ meV) vs squared electric field amplitude of $\lambda = 90.5$ μm radiation. The three sample temperatures are specified at the curves. The dashed straight lines are plots of the relation $e(E) \propto A \exp(E^2/E_c^2)$ constructed with the experimental values of τ_2, and the solid lines relate to the calculations made using Eqs. (28)–(32). The calculations made use of the experimental values of τ_2 and of the localized vibrational frequency $\omega = 2 \times 10^{13}$ s^{-1}.

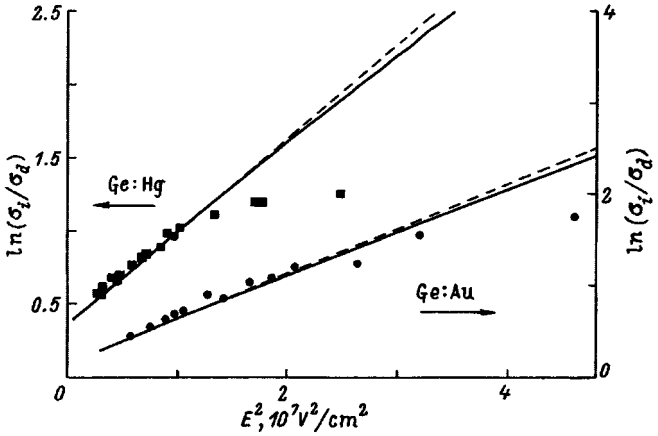

FIG. 18. Log conductivity ratio under illumination and in the dark, $\ln(\sigma_i/\sigma_d)$, of germanium samples doped with Au and Hg, obtained at $T = 46$ K *vs* squared electric field amplitude of $\lambda = 90.5$ μm radiation. The dashed lines are plots of the relation $e(E) \propto A \exp(E^2/E_c^2)$ constructed with the experimental values of τ_2, and the solid lines relate to the calculations made using Eqs. (28)–(32). The calculations made use of the experimental values of τ_2 and of the localized vibrational frequency $\omega = 2 \times 10^{13}$ s^{-1}.

at which $\varepsilon_m = \mathscr{E}_0$ is E_0, which is determined by Eqs. (24) and (25):

$$E \gg E_0 = \frac{2\omega\sqrt{2m^*\varepsilon_T}}{e}\omega\tau_2. \tag{58}$$

The ionization probability in the field domain defined by inequality (58), according to Ref. 96, is characterized by weaker field dependences [see Eqs. (26) and (27)]. The experimentally observed change in the character of the field dependence for fields corresponding in order of magnitude to the calculated values of E_0 permits a conclusion that for $E \gg E_0$ the mechanism of direct tunneling ionization becomes dominant.[108]

A general expression describing the limiting cases of both multiphonon and direct tunneling was obtained[90] within the Huang–Rhys model (see Sec. 1.4). Consider the results of calculating the field dependence of emission probability performed by using Eqs. (28)–(32) (see 1.4). The calculation makes use of three phenomenological parameters, namely, thermal ionization energy ε_T, localized vibrational frequency ω, and the nondimensional electron-phonon coupling constant $\beta = \Delta\varepsilon/\varepsilon_T$. The value of thermal ionization energy ε_T was taken from literature. The tunneling times τ_2 (Fig. 15) were then used to determine the tunneling time τ_1 which, according to Eqs. (2) and (15), relates parameter β to the localized vibrational frequency ω. Thus the problem reduces to finding the only fitting parameter, for which the localized vibrational frequency was taken. Its value ($\omega = 2 \times 10^{13}$ s^{-1}) determined for one temperature and one impurity was not changed in the subsequent treatment of the data obtained for other temperatures and other impurities in the same material, in other words, there were no fitting parameters after that. Figure 19 shows the calculated probabilities of emission in an electric field $e(E)$ normalized to that of thermal emission $e(0)$ for different localized vibrational frequencies ω. We see that the emission probability depends noticeably on ω for fields $E > E_0$ and, thus, ω can indeed be used as a fitting parameter.

Figures 16–18 compare the calculations made using Eqs. (28)–(32) (Sec. 1.4) with experimental data. We readily see that while the deviation from the $e(E) \propto \exp(E^2/E_c^2)$ relation observed for $E > E_0$ is described satisfactorily by theory, the latter gives a stronger dependence on intensity than the one measured in experiment. We note also that the characteristic electric field E_0 as a function of temperature and thermal ionization energy is in a good agreement with theory for all

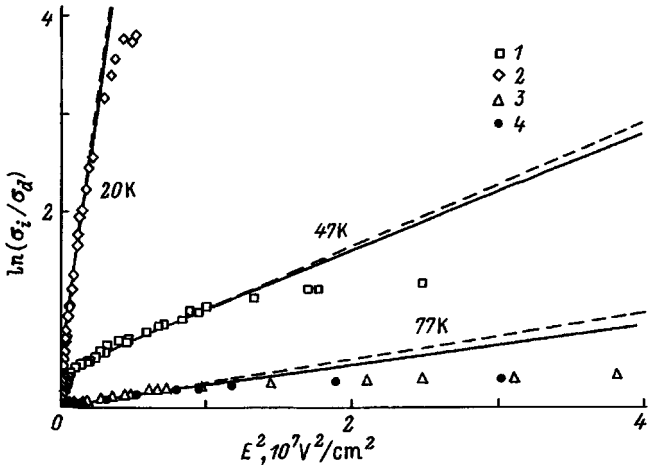

FIG. 17. Log conductivity ratio under illumination and in the dark, $\ln(\sigma_i/\sigma_d)$, of Hg-doped germanium samples ($\varepsilon_T = 90$ meV) vs squared electric field amplitude of radiation with λ(μm): (*1–3*) 90.5 and (*4*) 250. The corresponding temperatures are specified at the curves. The dashed lines are plots of the relation $e(E) \propto A \exp(E^2/E_c^2)$ constructed with the experimental values of τ_2, and the solid lines relate to the calculations made using Eqs. (28)–(32). The calculations made use of the experimental values of τ_2 and of the localized vibrational frequency $\omega = 2 \times 10^{13}$ s^{-1}.

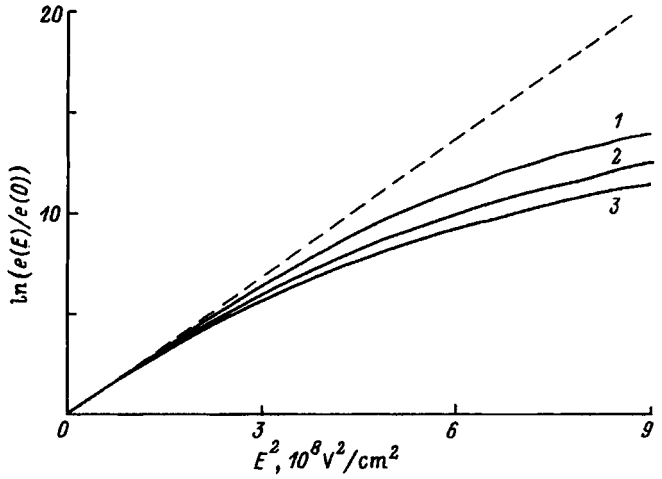

FIG. 19. Log probability ratio of ionization in an electric field to thermal ionization, $\ln[e(E)/e(0)]$, for Hg-doped germanium ($\varepsilon_T = 90$ meV) vs squared electric-field amplitude calculated for different localized vibrational frequencies for $T = 77$ K using Eqs. (28)–(32). $\omega(10^{13}\ \mathrm{s}^{-1})$: *1*—6, *2*—4, *3*—3.

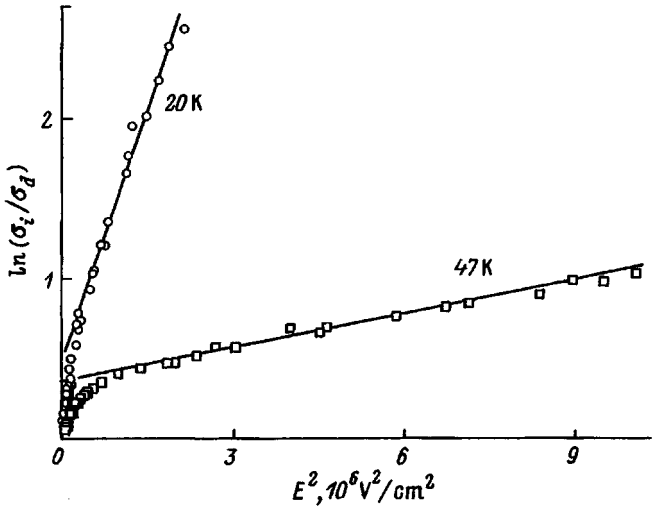

FIG. 20. Log conductivity ratio under illumination and in the dark, $\ln(\sigma_i/\sigma_d)$, of Hg-doped germanium samples *vs* squared electric-field amplitude of $\lambda = 90.5$ μm radiation. The corresponding temperatures are specified at the curves.

the studied impurities exhibiting weak electron-phonon coupling.

One of the reasons for the discrepancy between theory and experiment in the high electric-field domain may be the scattering of tunneling carriers under the barrier, which sets an upper bound for the tunneling probability. This process was considered for carrier tunneling through Schottky barriers,[117] where the observed tunneling probability was also smaller than that predicted by theory. The energy of the tunneling electron ε_m and the length of the under-barrier tunneling trajectory increase with electric field to the extent where the scattering processes place a limit on the emission.

4.3. Charge effect and the Poole–Frenkel effect

In the region of relatively weak electric fields one also observes deviations from the $\exp(E^2/E_C^2)$ behavior, clearly seen in Fig. 20 displaying the $\ln(\sigma_i/\sigma_d)$ *vs* E^2 relation for Ge:Hg. The dominant mechanism in this ionization process is the Poole–Frenkel effect (see Sec. 1.5), which is seen in the onset of an exponential dependence of photoresponse signal on the square root of electric field, $e(E) \propto \exp\sqrt{E/E_{PF}}$. Data for the weak-field region are shown in Figs. 21 and 22, where $\ln(\sigma_i/\sigma_d)$ is plotted as a function of the square root of the high-frequency electric-field amplitude, $\sqrt{E}$. In the low-field domain, the ionization probability is seen to grow strongly with decreasing temperature, following closely the $e(E) \propto \exp\sqrt{E/E_{PF}}$ relation. The square-root dependence of $\ln(\sigma_i/\sigma_d)$ on E and its temperature behavior are in good agreement with Eqs. (33) and (34) describing the Poole–Frenkel effect.

At the same time the theory of Frenkel does not provide an adequate description of the dependence of conductivity on the high-frequency electric field. The slope of the dependence of $\ln(\sigma_i/\sigma_d)$ on the square root of electric field is about one half that calculated from Eqs. (33) and (34), which may also may be considered as an argument for the presence of multiphonon processes (Sec. 1.5). For low fields, the conductivity does not vary at all (Fig. 22). The same deviations from Eqs. (33) and (34) are observed also in the case of dc fields[83] and accord with published data.[83,118–122]

The charge effect manifests itself also in multiphonon tunneling ionization, resulting, according to Eq. (36), in an additional factor in the ionization probability. This is seen

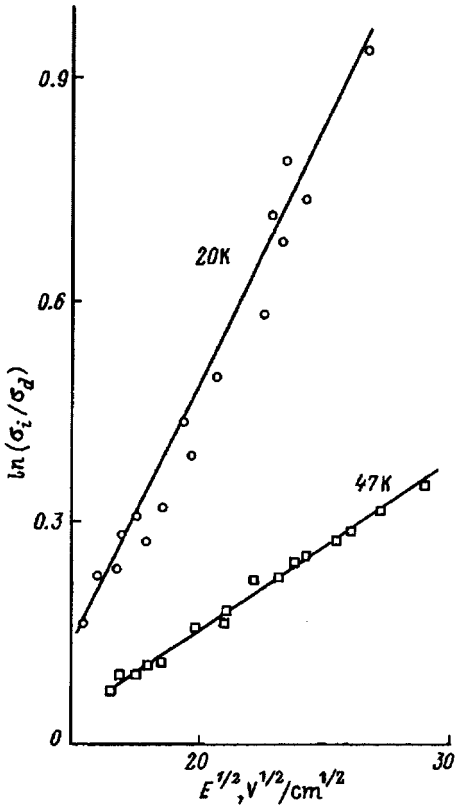

FIG. 21. Log conductivity ratio under illumination and in the dark, $\ln(\sigma_i/\sigma_d)$, of Hg-doped germanium samples *vs* square root of the electric-field amplitude of $\lambda = 90.5$ μm radiation. The corresponding temperatures are specified at the curves.

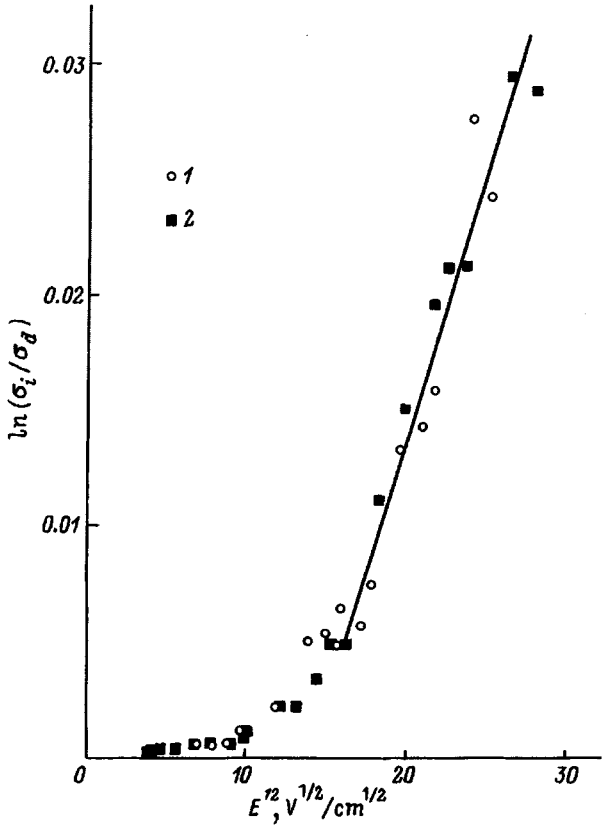

FIG. 22. Log conductivity ratio under illumination and in the dark, $\ln(\sigma_i/\sigma_d)$, of Hg-doped germanium samples at 77 K *vs* square root of the radiation electric-field amplitude. The data are presented for different wavelengths of the exciting radiation. $\lambda(\mu m)$: (*1*) 90.5, (*2*) 250.

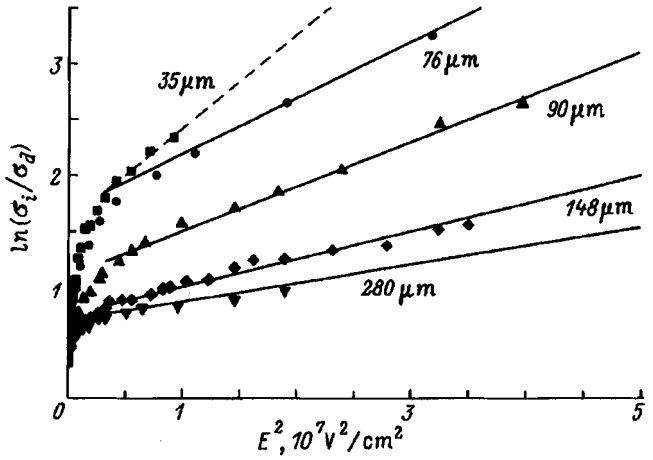

FIG. 23. Log conductivity ratio under illumination and in the dark, $\ln(\sigma_i/\sigma_d)$, of Hg-doped germanium samples *vs* squared electric-field amplitude of $\lambda = 90.5$ μm radiation obtained at 40 K for different wavelengths of exciting radiation (specified at the curves). The straight lines plot relation $e(E) \propto A \exp(E^2/E_c^2)$ with E_c^2 used as a fitting parameter.

from extrapolation of the straight lines corresponding to the region of multiphonon tunneling ionization to zero electric field. We see that $\ln(\sigma_i/\sigma_d)$ does not vanish for $E=0$ (Figs. 12 and 20), which implies that σ_i is not equal to σ_d, as this followed from Eq. (23) which does not take into account the charge effect.

4.4. Effects due to the high-frequency of FIR radiation

As shown in the preceding Sections, ionization of deep impurity centers by FIR-SBM radiation is a result of tunneling processes occurring in the wave electric field. The ionization probability here does not depend on radiation frequency, and the action of the high-frequency field is equivalent to application of a strong electric field across the sample. As pointed out in Sec. 1.6, however, an increase in radiation frequency or decrease of sample temperature, i.e. transition to the condition $\Omega\tau_2 = \Omega(\hbar/2k_BT + \tau_1) > 1$, should result in the ionization probability becoming dependent on frequency. The frequency dependence of ionization probability was measured in Ge:Hg samples ($\varepsilon_T = 90$ meV).

The results obtained at $T=40$ K and at wavelengths from 35 to 280 μm are presented graphically in Fig. 23. It is seen that the photoresponse signal grows substantially with radiation frequency while retaining at the same time the character of the field dependence $\ln(\sigma_i/\sigma_d) \propto \exp(E^2/E_c^2)$. The same sample does not exhibit any frequency dependence at higher frequencies (Fig. 9).

Experiments showed that within this frequency range the $\ln(\sigma_i/\sigma_d) \propto \exp(E^2/E_c^2)$ relation, which is typical of multiphonon tunneling, occurs above 30 K. For lower temperatures, the frequency dependence becomes stronger, and the electric field dependence of the photoresponse signal changes its character.

The field dependence of the ionization probability measured for Ge:Hg within the temperature range $T=35-80$ K and at wavelengths $\lambda = 35-280$ μm was used to derive the effective tunneling time τ_2^* (see Sec. 1.6). Figure 24 displays the dependence of the ratio τ_2^*/τ_2, where τ_2 is the tunneling time in a dc electric field, as a function of parameter $\Omega\tau_2$ which is dominant in the frequency effects. The tunneling time τ_2 was derived from measurements at the longest wavelengths, where no frequency dependence is observed. We see that $\tau_2^* = \tau_2$ up to $\Omega\tau \simeq 1$, in support of the conclusion that the radiation field acts in this region as a dc field (all the experiments quoted here before were done with this condition met). An increase of $\Omega\tau_2$, which corresponds to an increase of frequency or decrease of temperature [see Eq. (12)], brings about a substantial increase in the effective tunneling time compared to the tunneling time τ_2. Figure 24 presents also the τ_2^*/τ_2 ratio as a function of $\Omega\tau_2$ calculated using Eq. (56). The theory of multiphonon-assisted tunneling (Sec. 1) is seen to agree well with experimental data.

As already pointed out, the theory of multiphonon tunneling in dc and high-frequency fields is valid provided electron tunneling contributes little to thermal emission. This is true if the electron tunneling energy ε_m is much smaller than the energy of defect tunneling, $\mathscr{E}_0$, and that of thermal ionization, ε_T. At low temperatures this condition breaks down because of the smallness of the optimum defect-tunneling energy, and, hence, the existing theory is inapplicable already for very low electric fields. Presented in Fig. 25 is a calculated dependence of the boundary beyond which the theory of multiphonon tunneling energy is no longer valid, as determined by the condition $\mathscr{E}_0/\varepsilon_m = 1$, on electric field

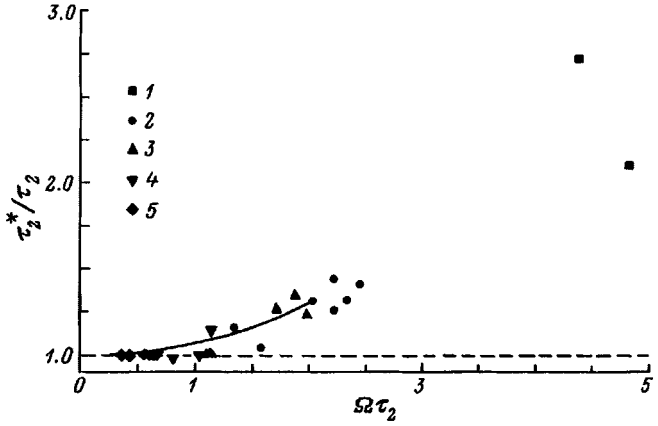

FIG. 24. Ratio of effective tunneling time, τ_2^*, to tunneling time in a dc field, τ_2, vs $\Omega\tau_2$, obtained from the field dependence of the ionization probability, which was determined for Ge:Hg in the temperature interval $T=35-80$ K and wavelength range $\lambda=35-280$ μm. $\lambda(\mu\text{m})$: (*1*) 35, (*2*) 76, (*3*) 90.5, (*4*) 148, and (*5*) 280. The solid line is constructed using Eq. (56).

strength E, temperature T, and radiation frequency Ω for Ge:Hg.

5. KINETIC STUDIES OF THE LONG-LIVED COULOMB EXCITED STATES OF A SHALLOW IMPURITY CENTER

Development of sources capable of generating short FIR-SBM pulses permitted study of the dynamics of nonequilibrium processes in semiconductors and semiconductor quantum-well structures.[21,40,123–126]

In the case of interest to us here, using short pulses for the ionization of impurities also makes possible the use of tunneling ionization in the FIR-SBM field to study carrier trapping by impurities. As pointed out in Sec. 2, the kinetics of the photoresponse observed are in agreement with the capture cross sections by an impurity which were obtained by other techniques for the materials under study.

Studies of the kinetics of the extrinsic photoconductivity occurring under multiphonon tunneling ionization of a shallow donor center (tellurium) in GaP in an electric field of pulsed laser radiation in the FIR range revealed specific features in the kinetics of carrier trapping and buildup in the valley-orbit split $1s(E)$ state of the shallow donor level.[127] Such long-lived excited electronic states were discovered earlier in simple substitutional impurities in Ge and Si from modulation of the microwave absorption[128,129]

We also consider here carrier buildup in the excited Te level in GaP under ionization of the impurity by short FIR-SBM pulses.

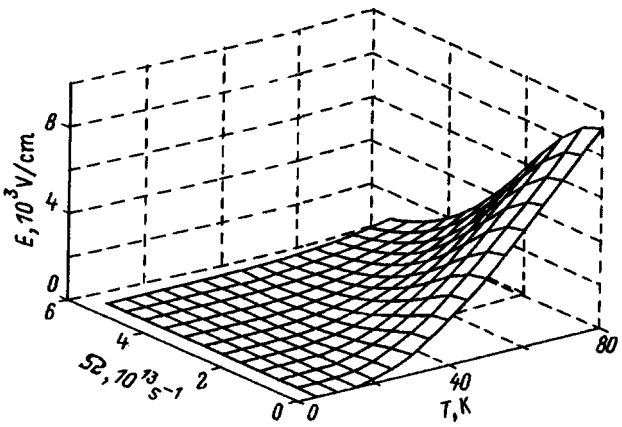

FIG. 25. Calculated boundary of applicability of multiphonon tunneling theory determined from condition $\mathscr{E}_0/\varepsilon_m=1$ vs electric field amplitude E, temperature T, and radiation frequency Ω for Ge:Hg.

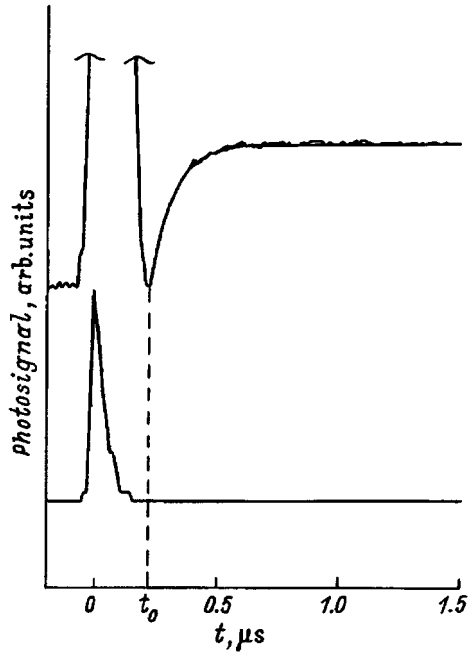

FIG. 26. Oscillographic trace of the photoresponse signal from a GaP:Te sample at $T=50$ K (upper curve) and of the exciting pulse with $\lambda=90.5$ μm recorded with a phonon-drag detector (lower curve). The smooth curve for the time interval $t>t_0$ is obtained using Eq. (64) with two fitting parameters, $1/\tau_{d1}=10^7$ s^{-1} and $1/\tau_{d2}=2.4\times10^3$ s^{-1}.

5.1. Experimental investigation of the trapping kinetics into shallow donor states of Te in GaP

Submillimeter photoconductivity measurements were carried out on GaP samples, which were doped heavily by tellurium to concentrations of 3×10^{17} and 7×10^{17} cm^{-3} and lightly compensated. The samples were maintained in an optical cryostat with the temperature variable from 20 to 150 K, where most of the carriers at thermal equilibrium are frozen out onto the ground-state impurity.

Illumination of a sample by FIR-SBM pulses increased its conductivity. Measurements of the photoresponse signal *vs* wavelength, radiation intensity, and temperature show that the ionization probability does not depend on wavelength and grows nonlinearly with the electric field E of the radiation as $\exp(E^2/E_c^2)$ while the characteristic field E_c^2 decreases with decreasing temperature as T^3, which implies that the ionization is produced by multiphonon-assisted tunneling in the electric field of the laser radiation.[127]

Figures 26 and 27 present typical photoresponse pulse shapes obtained in different time intervals. Shown in Fig. 26 is the photoresponse of the sample measured during the laser pulse and immediately after its completion, to be compared with the laser pump pulse registered by a photon-drag detec-

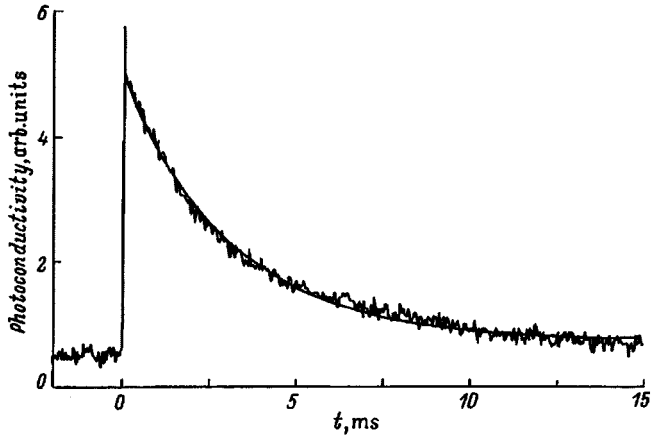

FIG. 27. Oscillographic trace of a photoresponse signal obtained from a Ga:P sample at $T=30$ K. The smooth curve for the time interval $t>t_0$ is obtained using Eq. (64) with two fitting parameters, $1/\tau_{d1}=10^7$ s^{-1} and $1/\tau_{d2}=2.5\times10^2$ s^{-1}.

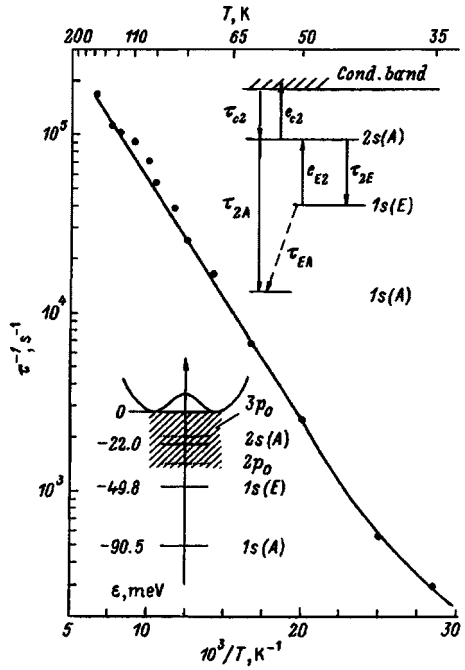

FIG. 28. Temperature behavior of the reciprocal photoconductivity-decay time, $1/\tau_1$, in GaP:Te. The curve plots $1/\tau_1=1/\tau_0[\exp(-\Delta\varepsilon/kT)+1.44\times10^2]$s^{-1} and $\Delta\varepsilon=28$ meV. The insets show schematically the camel-back structure of the conduction band and the energy position of the ground and of a number of the lowest excited states of Te in GaP constructed in accordance with Ref. 135 (bottom left corner), and the kinatic model of relaxation (top right corner).

tor. The first fast photoresponse component is clipped to demonstrate more clearly the unusual behavior of the response after the radiation pulse. The response is seen to grow during the radiation pulse and subsequently drop to zero in times shorter than 40 ns. After the end of the pulse, however (for $t>t_0$), the signal starts to grow again and reaches a maximum in one microsecond, to finally fall off exponentially to zero (Fig. 27). The signal growth after the end of the pulse can be fitted well by the function $a[1-\exp((t-t_0)/\tau_r)]$, with a characteristic time τ_r of the order of 10^{-7} s. The characteristic time of the subsequent slow exponential decay τ_1 does not depend on the intensity and frequency of the radiation but is strongly temperature dependent, increasing by nearly three orders of magnitude with the temperature decreasing from 150 K (6 μs) to 35 K (3 ms). Figure 28 presents the reciprocal decay time, $1/\tau_1$, as a function of inverse temperature. This strong temperature dependence can be well fitted in a first approximation by the function $1/\tau_1=1/\tau_0\ \exp(-\Delta\varepsilon/kT)$ with $\Delta\varepsilon=28$ meV.

The fast component of the signal is accounted for by ionization and fast capture into the excited Coulomb states of tellurium.[130,131] The main difficulty consists here in explaining the growth and decay of the signal after the end of the radiation pulse.

The heating of the electron gas or of the sample as a whole can be excluded as possible formation mechanisms of the photoconductive signal. It was shown[132,133] that at 70 K and higher the electron mobility and, hence, conductivity in GaP decreases with increasing temperature. Thus observation of positive photoconductivity excludes electron gas heating by radiation as a possible cause of the photoresponse. Besides, heating of the sample cannot account for the complex time behavior of the slow signal component and the detected increase of the exponential decay time constant by three orders of magnitude with the temperature changing by five times only.

Presence of additional deep impurities, for instance, of oxygen, which has a small capture cross section (10^{-22} cm^2, Ref. 134) cannot explain the observed kinetics of the photoresponse signal. To obtain the measured long decay time by this mechanism, one would have to assume that the concentration of oxygen in the sample is comparable to that of tellurium, 5×10^{17} cm^{-3}, which contradicts the low level of light compensation in the material under study.

5.2. Kinetic model of the relaxation process in the presence of a long-lived excited state

The initial fast decay of the photoconductive signal is due to the fast cascade trapping of free carriers into high excited states, which subsequently relax to the ground state. The latter stage requires essentially a longer time because of the large energy gap between the excited Coulomb states and the ground state. In the case of deep centers[1)] it usually occurs through multiphonon-assisted processes or optical transitions. The dynamic time consists in this case of two components, namely, a fast and a slower one. The slow decay time is, however, either temperature-independent or grows with temperature, which is at odds with experiment.[75] Thus the cascade trapping model, unless it is modified properly, cannot account for the increase of the photoconductive signal after the end of the pulse, and the observed temperature behavior of the slow signal decay.

We are going to show that the assumption of the existence of a long-lived excited state characterized by an extremely small transition probability to the ground state permits one to describe adequately the kinetics of the observed signal. The carriers build up in this state and return later by thermal activation to an array of closely spaced Coulomb

states located near the bottom of the conduction band, thus increasing the carrier concentration in the conduction band accordingly.

The inset to Fig. 28 shows a characteristic camel-back-shaped structure of the conduction-band bottom and the position of the ground state and of a number of the lowest excited states of Te in GaP, constructed in accordance with Ref. 135. We readily see that valley-orbit coupling splits the $1s$ state in GaP into two states [$1s(E)$ and $1s(A)$] separated by a gap of 40.7 meV. Cascade trapping was shown[75] to occur primarily over the s states by one-phonon acoustic transitions. Since the energy gap between the $1s(E)$ and the ground state exceeds by far the maximum energy of the acoustic phonon (31.5 meV, Ref. 135) while being less than that of the optical phonon (51 meV by Ref. 135), the electrons promoted to the $1s(E)$ level cannot transfer to the ground state by one-phonon processes, which results in their buildup in this level. The most probable relaxation channel from this state is one-phonon excitation into the next, higher lying s state, $2s(A)$, separated from $1s(E)$ by 28 meV. Note that the exponential dependence of the slow-decay time τ_1 on temperature is characterized by an energy of 28 meV. One may thus conjecture that electrons build up in the $1s(E)$ state, are promoted by thermal excitation to the $2s(A)$ state, and transfer to the closely lying p states through absorption and emission of acoustical phonons, to relax finally via optical (infrared) transitions to the ground state. The kinetic model based on these assumptions is presented schematically in the upper right corner of Fig. 28.

For $t>t_0$, when there is no generation of nonequilibrium carriers, the rate equations determining the electron concentrations n in the conduction band and the concentrations n_2 and n_E in the $2s(A)$ and $1s(E)$ states can be written

$$\frac{dn}{dt}=-\frac{n}{\tau_{c2}}+e_{2c}n_2,$$

$$\frac{dn_2}{dt}=\frac{n}{\tau_{c2}}-e_{2c}n_2-\frac{n_2}{\tau_{2E}}+e_{E2}n_E-\frac{n_2}{\tau_{2A}},$$

$$\frac{dn_E}{dt}=\frac{n_2}{\tau_{2E}}-e_{E2}n_E-\frac{n_E}{\tau_{EA}}. \tag{59}$$

We have neglected here the thermal population of the states and introduced the following characteristic transition times: τ_{c2}-from the conduction band to the $2s(A)$ level, τ_{2E} and τ_{2A}-from $2s(A)$ to the $1s(E)$ and $1s(A)$ level, respectively, and τ_{EA}-from the $1s(E)$ to $1s(A)$ level. The probabilities of the reverse processes, e_{2c} and e_{E2}, are related through the principle of detailed balance to the τ_{c2} and τ_{2E} times, respectively. For instance, for the transition probability e_{E2}, which is essential for the model, we obtain

$$e_{E2}=\frac{1}{\tau_{2E}}\exp(-\Delta\varepsilon_{2E}/k_{\mathrm{B}}T), \tag{60}$$

where $\Delta\varepsilon_{2E}$ is the energy separation between the $1s(E)$ and $2s(A)$ levels.

The first of Eqs. (59) shows that for $t>t_0,\tau_{c2}$ a quasi-equilibrium sets in between the electrons in the conduction band and those populating the $2s(A)$ state, i.e. $n=e_{2c}\tau_{c2}n_2$. In these conditions, concentration n_2 determines the concentration n of nonequilibrium free carriers in the conduction band and, thus, the photoresponse signal. Substituting $n=e_{2c}\tau_{c2}n_2$ in Eq. (59) reduces the set of three equations to a set of the two latter equations for $t>t_0$. Then the electron concentration in the $2s(A)$ state as a function of time can be written

$$\begin{aligned}n_2(t)=&\frac{1}{\left(\frac{1}{\tau_{d1}}-\frac{1}{\tau_{d2}}\right)}\left\{\left[n_2^{(0)}\left(\frac{1}{\tau_{2A}}+\frac{1}{\tau_{2E}}-\frac{1}{\tau_{EA}}\right.\right.\right.\\&\left.-e_{2c}\frac{\tau_{2E}}{(\tau_{2A}+\tau_{2E})}\right)-e_{E2}n_E^{(0)}\left.\right]\exp\left(-\frac{(t-t_0)}{\tau_{d1}}\right)\\&+\left[e_{E2}n_2^{(0)}\frac{\tau_{2A}}{(\tau_{2A}+\tau_{2E})}+e_{E2}\cdot n_E^{(0)}\right]\\&\left.\times\exp\left(-\frac{(t-t_0)}{\tau_{d2}}\right)\right\},\end{aligned} \tag{61}$$

where $n_2^{(0)}$ and $n_E^{(0)}$ are the concentrations in states $2s(A)$ and $1s(E)$ at time $t=t_0$, respectively, and τ_{d1} and τ_{d2} are the dynamic relaxation times defined by

$$\frac{1}{\tau_{d1}}=\frac{1}{\tau_{2A}}+\frac{1}{\tau_{2E}}+e_{E2}\frac{\tau_{2A}}{(\tau_{2A}+\tau_{2E})}, \tag{62}$$

$$\frac{1}{\tau_{d2}}=e_{E2}\frac{\tau_{2E}}{(\tau_{2A}+\tau_{2E})}+\frac{1}{\tau_{EA}} \tag{63}$$

Assuming $\tau_{2E}\ll\tau_{2A}$ we come to the inequality $n_E^{(0)}\gg_2^{(0)}$. Neglecting in Eq. (61) terms proportional to $n_2^{(0)}$ compared to those proportional to $n_E^{(0)}$ one obtains

$$n_2(t)\approx\frac{e_{E2}n_E^{(0)}}{\left(\frac{1}{\tau_{d1}}-\frac{1}{\tau_{d2}}\right)}\left[\exp\left(-\frac{(t-t_0)}{\tau_{d2}}\right)-\exp\left(-\frac{(t-t_0)}{\tau_{d1}}\right)\right]. \tag{64}$$

For $\tau_{d1}<\tau_{d2}$, Eq. (64) shows n_2 to vary nonmonotonically with time, namely, after the removal of illumination n_2 exhibits a growth followed by an exponential decay. Figures 26 and 27 compare the evolution of carrier concentration in the conduction band, which determines the photoresponse kinetics and was calculated using Eq. (61), with experiment. The times τ_{d1} and τ_{d2} were taken as fitting parameters. Since these times differ by at least two orders of magnitude, one actually used only one fitting parameter in each time interval. The dynamic times determined in this way are: $1/\tau_{d1}=10^7\ \mathrm{s}^{-1}$ and $1/\tau_{d2}=[1.6\times10^6\exp(\Delta\varepsilon_{2E}/k_BT)+1.44\times10^2]\mathrm{s}^{-1}(\Delta\varepsilon_{2E}=28\ \mathrm{meV})$. Figure 28 presents calculated τ_{d2} times (solid line) to be compared with the experimentally determined slow decay time as a function of temperature. The results of a numerical calculation are seen to be in good agreement with experiment.

It can be shown that, within the temperature interval under consideration, the last term in Eq. (62) is much smaller than the sum of the first two terms, $1/\tau_{2A}+1/\tau_{2E}$. Neglecting it in Eq. (62), we find from the experimentally measured dynamic times and the temperature dependence of τ_{d2} the three characteristic times introduced earlier: $\tau_{2E}=10^{-7}$ s,

$\tau_{2A}=5\times10^{-7}$ s, and $\tau_{EA}=0.7\times10^{-2}$ s. These values accord with the condition $\tau_{2E}<\tau_{2A}\ll\tau_{EA}$ used in the calculation.

Thus investigation of the kinetics of FIR–SBM-induced photoconductivity in GaP:Te permitted observation of the buildup of electrons in the excited state of a shallow donor level in times up to a few milliseconds, and its identification as a valley-orbit split $1s(E)$ state. Electrons are promoted from this state by thermal excitation into the higher-lying s and p states, with subsequent relaxation to the ground state occurring primarily by radiative transitions. The existence of radiative transitions was established here through observation of infrared luminescence.[127]

6. CONCLUSIONS

Photoionization of deep impurity centers in semiconductors stimulated by high-intensity submillimeter laser radiation having photon energies much smaller than the impurity ionization energy has been discovered and studied within a broad range of intensities, wavelengths, and temperatures, and for a variety of impurities. A comprehensive comparison of experimental data with the theory of multiphonon-assisted and direct deep-impurity ionization in an electric field has shown that terahertz radiation acts frequently like a dc field.

Within a broad electric-field range, the carrier emission probability can be described in terms of multiphonon-assisted tunneling. Thermally activated emission of carriers from the ground state to continuum is usually accompanied by thermal excitation of the system followed by tunneling of the defect from the configuration corresponding to a bound electron state to that of an ionized impurity. Electric field enhances defect tunneling by the electrons tunneling through the barrier produced by the electronic potential and the electric field. This enhancement of carrier emission was detected from the photoconductive signal. The field dependence of this signal permitted one to determine the defect tunneling times. The self-trapped character of the impurity center can be established unambiguously by comparing the tunneling time with the reciprocal temperature multiplied by a combination of universal constants (namely, $\hbar/2k_BT$).

For relatively weak and very strong fields, the observed probability of ionization differs from that of multiphonon tunneling. In the weak-field domain, the impurity ionization is produced by the Poole–Frenkel effect, which results from lowering the energy of thermal ionization of attractive centers. In strong fields, ionization occurs by direct tunneling without thermal activation. The proposed method of impurity ionization by short FIR-SBM laser pulses permits contactless application of very strong electric fields to a sample and, thus, helps one to avoid problems associated with the onset of avalanche breakdown, current pinching etc., which are frequently encountered when operating with strong static electric fields. The high sensitivity of the photoresponse offers a possibility of measurements over a broad field range, from very low intensities to tens of kV per cm.

APPENDIX EFFECTS OF RADIATION HEATING

Absorption of high-power FIR–SBM radiation by free carriers results in a strong heating of the electron gas. In the experiments considered here, there are practically no free carriers, which is a condition of weak absorption, and therefore the heating of the electron gas and of the lattice is small. Our analysis would not, however, be complete without an assessment of the possible contribution of heating processes to photoconductivity.

The variation of sample conductivity caused by electron gas heating under FIR illumination is due to the change in the mobility of the carriers as a result of the change in their energy distribution. This process is well known and was thoroughly studied on a variety of materials, namely, InSb, GaAs, Ge, etc. If the free-carrier concentration is large enough, the heating process can be described in terms of the electron temperature T_e, whose variation is determined by the absorption of radiation. In the FIR region, for $\hbar\Omega\ll\hbar\omega_0$, where $\hbar\omega_0$ is the optical phonon energy, the electron temperature is found from the balance equation:

$$\alpha I\hbar\Omega=P_{\rm ac}(T_e)+P_{\rm opt}(T_e), \tag{A1}$$

where α is the coefficient of absorption by free carriers, and $P_{\rm ac}(T_e)$ and $P_{\rm opt}(T_e)$ are, respectively, the energy losses due to scattering from acoustic and optical phonons (see, e.g., Refs. 136–142). The energy contribution determining the photoconductive signal due to heating (both linear and nonlinear) depends on the absorption of radiation and, hence, on the free-carrier concentration.

If the heating is weak, the radiation-induced variation of the conductivity can be well approximated by a simple expression

$$\frac{\Delta\sigma}{\sigma}=\frac{1}{\mu}\frac{\partial\mu}{\partial T_e}\bigg|_{T_e=T_0}\Delta T_e, \tag{A2}$$

where T_0 is the lattice temperature.

We readily see that the sign of the photoconductive signal is determined by that of the derivative $\partial\mu/\partial T_e$. It is well known that this sign can be positive (for instance, if scattering from charged impurities is dominant) or negative (in the case where scattering occurs predominantly from acoustical phonons, optical phonons, etc.).[141,143]

The main experiments of deep-impurity ionization were performed using germanium samples. To reveal the role heating processes play in the submillimeter-range photoconductivity observed in samples having deep impurities, a study was carried out of the electron gas heating in Ge doped with shallow impurities (Ga,Sb) at close to liquid-nitrogen temperature, where the impurities are ionized, i.e. under the conditions most favorable for the heating. The concentrations were chosen close to those of deep impurities in the samples considered in this work.

Free-carrier heating in Ge in the temperature interval of interest results in negative photoconductivity, since the major part here is played by scattering by acoustic phonons, which brings about a decrease of the mobility with increasing electron-gas temperature. The kinetics of the photoconductivity caused by the free-carrier heating is dominated by

the short times of the free- carrier energy relaxation, which lie usually in the range $10^{-9}-10^{-13}$ s. Accordingly, the signals generated by electron heating either repeat the radiation pulse in shape or exhibit a more complex behavior in time, but do not exceed in duration the nanosecond-range excitation pulses.

Thus observation of positive photoconductivity in samples containing less than 5×10^{14} cm^{-3} deep impurities at $T\simeq77$ K during times longer than the radiation pulse duration exclude electron gas heating as a possible cause of the photoresponse. This is accounted for by the suppression of heating in samples doped primarily by deep impurities and maintained at sufficiently low temperatures by carrier freezeout at the impurity and, hence, a practically complete absence of absorption.

Note that the free-carrier concentration in $Al_xGa_{1-x}Sb$ and $Al_xGa_{1-x}As$ samples in which DX centers were studied was high enough for the heating effects to provide a substantial contribution to photoresponse. The strong difference between the relaxation times of the heating-induced photoconductivity and of the photoconductivity due to the ionization of the DX centers permitted, however, easy separation of these contributions.

In the conditions of strong nonlinear carrier heating by high-intensity radiation one can observe also photoionization of deep impurities with light of $\hbar\Omega<\varepsilon_T$ in the course of light-induced impact ionization, first discovered in InSb.[34] In this case one detects, in addition to the prevailing fast μ photoresponse signals, positive photoconductivity, whose kinetics are dominated by the nonequilibrium-carrier lifetime. Since the carriers are heated here by the high-frequency field, the probability of the light-induced impact ionization falls off exponentially with increasing radiation frequency. The opposite frequency-dependence patterns of behavior exhibited by tunneling (multiphoton) and impact ionization permit one to identify the processes. Thus the absence of the fast negative component of μ photoconductivity in the positive photoresponse signal observed under high-intensity FIR illumination in samples having deep impurities, as well as the independence of probability on wavelength, or its decrease with the latter, gives us grounds for an unambiguous exclusion of light-induced impact ionization from among the processes which could be responsible for the deep-impurity ionization discussed in the present work.

In conclusion, consider the possible effect of lattice heating. Similarly to the case of electron gas heating, heating of the lattice by radiation should affect the conductivity. In this case, the sign of the photoconductivity is determined by both the variation of mobility (the carriers are ionized) and an increase of carrier concentration in the band (the carriers are frozen out at the impurity). The kinetics of photoconductivity are dominated in this case by the slow cooling of the sample as a whole (on a time scale substantially longer than microseconds). Observation in samples containing deep impurities of signals with characteristic times of the order of a few microseconds and shorter gives one grounds to exclude the heating of the sample as a whole as the cause of the photoresponse. We also note that no lattice heating effects were observed in the bulk semiconductors illuminated by short (100 ns) radiation pulses having energies not in excess of a mJ, even at high free-carrier concentrations (see, for instance, Refs. 39–41, 43, 114).

The authors are grateful to Deutsche Forschungsgesellschaft for support of the work and to V. I. Perel' for numerous fruitful discussions.

*Present address: A. F. Ioffe Physicotechnical Institute, Russian Academy of Sciences, 194021 St. Petersburg, Russia.

[1)]Although tellurium is a donor center, its ground-state energy is farly high (90 meV).

[1] T. Y. Chang and T. J. Bridges, Opt. Commun. **1**, 423 (1970).
[2] Th. de Temple, in *Infrared and Millimeter Waves*, edited by K. J. Button, New York, Vol. 1, 129 (1979).
[3] L. R. Elias, J. Hu, and G. Ramian, Nucl. Instrum. Methods Phys. Res. A **237**, 203 (1985).
[4] L. R. Elias, G. Ramian, J. Hu, and A. Amir, Phys. Rev. Lett. **57**, 424 (1986).
[5] A. A. Andronov, in *Infrared and Millimeter Waves*, edited by K. J. Button, New York, Vol. 16, 150 (1986).
[6] L. E. Vorob'ev, F. I. Osokin, V. I. Stafeev, and V. N. Tulupenko, JETP Lett. **34**, 118 (1981).
[7] V. I. Gavrilenko, V. N. Murzin, S. A. Stoklitskiĭ, and A. P. Chebotarev, JETP Lett. **35**, 97 (1982).
[8] Yu. L. Ivanov and Yu. B. Vasil'ev, Pis'ma Zh. Tekh. Fiz. **9**, 613 (1983) [Sov. Tech. Phys. Lett. **9**, 264 (1983)].
[9] Yu. A. Mityagin, V. N. Murzin, O. N. Stepanov, and S. A. Stoklitsky, Phys. Scr. **49**, 699 (1994).
[10] I. V. Altukhov, M. S. Kagan, and V. P. Sinis, Opt. Quantum Electron. **23**, S211 (1991).
[11] S. D. Ganichev, S. A. Emel'yanov, and I. D. Yaroshetskiĭ, JETP Lett. **35**, 368 (1982).
[12] F. Keilmann, Infrared Phys. **31**, 373 (1991).
[13] W. Böhm, E. Ettlinger, and W. Prettl, Phys. Rev. Lett. **47**, 1198 (1981).
[14] S. D. Ganichev, S. A. Emel'yanov, E. L. Ivchenko, E. Yu. Perlin, and I. D. Yaroshetskiĭ, JETP Lett. **37**, 568 (1983).
[15] S. D. Ganichev, S. A. Emel'yanov, E. L. Ivchenko, E. Yu. Perlin, Ya. V. Terent'ev, A. V. Fedorov, and I. D. Yaroshetskiĭ, Zh. Eksp. Teor. Fiz. **91**, 1233 (1986) [Sov. Phys. JETP **64**, 729 (1986)].
[16] A. Avetissian, M. Hosek, and H. Minassian, Solid State Commun. **60**, 419 (1986).
[17] B. N. Murdin, C. R. Pidgeon, A. K. Kar, D. A. Jaroszynski, J. M. Ortega, R. Prazeres, F. Glotin, and D. C. Hutchings, Opt. Mater. **2**, 89 (1993).
[18] P. S. S. Guimarães, B. J. Keay, J. P. Kaminski, S. J. Allen, Jr., P. F. Hopkins, A. C. Gossard, L. T. Florez, and J. P. Harbison, Phys. Rev. Lett. **70**, 3792 (1993).
[19] B. Galdrikian, B. Birnir, and M. Sherwin, Phys. Lett. A **203**, 319 (1995).
[20] C. R. Pidgeon, A. Vass, G. R. Allan, W. Prettl, and L. Eaves, Phys. Rev. Lett. **50**, 1309 (1983).
[21] E. V. Beregulin, S. D. Ganichev, K. Yu. Glukh, and I. D. Yaroshetskiĭ, Fiz. Tekh. Poluprovodn. **21**, 1005 (1987) [Sov. Phys. Semicond. **21**, 615 (1987)].
[22] S. P. Lov and A. J. Sievers, in *Transport, Correlation, and Structural Defects*, edited by H. Fritzsche (World Scientific, Singapore, 1990).
[23] G. Jungwirt, R. Kropf, and W. Prettl, Int. J. Infrared Millim. Waves **12**, 729 (1991).
[24] R. Till and F. Keilmann, Phys. Rev. B **44**, 1554 (1991).
[25] F. Keilmann and R. Till, Opt. Quantum Electron. **23**, S231 (1991).
[26] F. Keilmann and R. Till, Semicond. Sci. Technol. **7**, 633 (1992).
[27] M. Helm, T. Fromherz, B. N. Murdin, C. R. Pidgeon, K. K. Geerinck, N. J. Hovenyer, W. Th. Wenckebach, A. F. G. van der Meer, and P. W. van Amersfoort, Appl. Phys. Lett. **63**, 3315 (1993).
[28] K. Craig, C. L. Felix, J. N. Heyman, A. G. Markelz, M. S. Sherwin, K. L. Campman, P. F. Hopkins, and A. C. Gossard, Semicond. Sci. Technol. **9**, 627 (1994).
[29] W. J. Li, B. D. McCombe, J. P. Kaminski, S. J. Allen, M. I. Stockman, L. S. Muratov, L. N. Pandey, T. F. George, and W. J. Schaff, Semicond. Sci. Technol. **9**, 630 (1994).
[30] P. M. Valov, B. S. Ryvkin, I. D. Yaroshetskiĭ, and I. N. Yassievich, Fiz. Tekh. Poluprovodn. **5**, 904 (1971) [Sov. Phys. Semicond. **5**, 797 (1971)].

[31] M. Weispfenning, I. Hoeser, W. Böhm, W. Prettl, and E. Schöll, Phys. Rev. Lett. **55**, 754 (1985).
[32] J. Kaminski, J. Spector, W. Prettl, and M. Weispfenning, Appl. Phys. Lett. **52**, 233 (1988).
[33] S. D. Ganichev, A. P. Dmitriev, S. A. Emel'yanov, Ya. V. Terent'ev, I. D. Yaroshetskiĭ, and I. N. Yassievich, JETP Lett. **40**, 948 (1984).
[34] S. D. Ganichev, A. P. Dmitriev, S. A. Emel'yanov, Ya. V. Terent'ev, I. D. Yaroshetskiĭ, and I. N. Yassievich, Zh. Éksp. Teor. Fiz. **90**, 445 (1986) [Sov. Phys. JETP **63**, 256 (1986)].
[35] A. Schilz, L. Huber, W. Prettl, and J. Kaminski, Appl. Phys. Lett. **60**, 2394 (1992).
[36] A. Mayer and F. Keilmann, Phys. Rev. B **33**, 6962 (1986).
[37] W. W. Bewley, C. L. Felix, J. J. Plombon, M. S. Sherwin, M. Sundaram, P. F. Hopkins, and A. C. Gossard, Phys. Rev. B **48**, 2376 (1993).
[38] M. Holthaus and D. W. Hone, Phys. Rev. B **49**, 16605 (1994).
[39] S. D. Ganichev, S. A. Emel'yanov, and I. D. Yaroshetskiĭ, JETP Lett. **38**, 448 (1983).
[40] E. V. Beregulin, S. D. Ganichev, K. Yu. Glukh, G. M. Gusev, Z. D. Kvon, M. Yu. Martisov, A. Ya. Shik, and I. D. Yaroshetskiĭ, JETP Lett. **48**, 269 (1988).
[41] E. V. Beregulin, S. D. Ganichev, K. Yu. Glukh, G. M. Gusev, Z. D. Kvon, A. Ya. Shik, and I. D. Yaroshetskiĭ, Zh. Éksp. Teor. Fiz. **97**, 2012 (1990) [Sov. Phys. JETP **70**, 1138 (1990)].
[42] J. Černe, A. G. Markelz, M. S. Sherwin, S. J. Allen, M. Sundaram, A. C. Gossard, P. C. van Son, and D. Bimberg, Phys. Rev. B **51**, 5253 (1995).
[43] I. N. Kotel'nikov, A. Ya. Shul'man, S. D. Ganichev, N. A. Varvanin, B. Mayerhofer, and W. Prettl, Solid State Commun. **97**, 827 (1996).
[44] N. G. Asmar, J. Černe, A. G. Markelz, E. G. Gwinn, M. S. Sherwin, K. L. Campman, and A. C. Gossard, Appl. Phys. Lett. B **68**, 829 (1996).
[45] A. A. Ignatov, E. Schomburg, K. F. Renk, W. Schatz, J. E. Palmier, and F. Mollot, Ann. Physik **3**, 137 (1994).
[46] K. Unterrainer, B. J. Keay, M. C. Wanke, S. J. Allen, D. Leonard, G. Medeiros-Ribeiro, U. Bhattacharya, and M. J. W. Rodwell, Phys. Rev. Lett. **76**, 2973 (1996).
[47] M. F. Kimmitt, F. I. M. Hammouda, and A. M. A. Assar, Infrared Phys. **23**, 63 (1983).
[48] S. D. Ganichev, S. A. Emel'yanov, and I. D. Yaroshetskiĭ, Fiz. Tekh. Poluprovodn. **17**, 698 (1983) [Sov. Phys. Semicond. **17**, 436 (1983)].
[49] S. D. Ganichev, S. A. Emel'yanov, Ya. V. Terent'ev, and I. D. Yaroshetskiĭ, Fiz. Tekh. Poluprovodn. **18**, 266 (1984) [Sov. Phys. Semicond. **18**, 164 (1984)].
[50] E. Garate, R. Cook, C. Shaughnessy, G. Boudreaux, and J. Walsh, Int. J. Infrared Millim. Waves **7**, 1827 (1986).
[51] M. F. Kimmitt, C. R. Pidgeon, D. A. Jaroszynski, R. J. Bakker, A. F. G. van der Meer, and D. Oepts, Int. J. Infrared Millim. Waves **13**, 1065 (1992).
[52] S. D. Ganichev, E. L. Ivchenko, R. Ya. Rasulov, I. D. Yaroshetskiĭ, and B. Ya. Averbukh, Fiz. Tverd. Tela (St. Petersburg) **35**, 198 (1993) [Phys. Solid State **35**, 104 (1993)].
[53] G. M. Gusev, Z. D. Kvon, L. I. Magarill, A. M. Palkin, V. I. Sozinov, O. A. Shegaĭ, and M. V. Éntin, JETP Lett. **46**, 33 (1987).
[54] E. V. Beregulin, S. D. Ganichev, K. Yu. Glukh, Yu. B. Lyanda-Geller, and I. D. Yaroshetskiĭ, Fiz. Tverd. Tela (Leningrad) **30**, 730 (1988) [Sov. Phys. Solid State **30**, 418 (1988)].
[55] E. V. Beregulin, S. D. Ganichev, K. Yu. Glukh, Yu. B. Lyanda-Geller, and I. D. Yaroshetskiĭ, Fiz. Tverd. Tela (Leningrad) **31**, 115 (1989) [Sov. Phys. Solid State **31**, 63, (1989)].
[56] E. V. Beregulin, S. D. Ganichev, K. Yu. Glookh, Yu. B. Lyanda-Geller, and I. D. Yaroshetskiĭ, Crystal Prop. Prepar. **19**, 327 (1989).
[57] E. V. Beregulin, S. D. Ganichev, K. Yu. Glukh, Yu. B. Lyanda-Geller, and I. D. Yaroshetskiĭ, Fiz. Tverd. Tela (St. Petersburg) **35**, 461 (1993) [Phys. Solid State **35**, 238 (1993)].
[58] S. D. Ganichev, I. N. Kotel'nikov, N. A. Mordovets, A. Ya. Shul'man, and I. D. Yaroshetskiĭ, JETP Lett. **44**, 301 (1986).
[59] S. D. Ganichev, K. Yu. Glukh, N. A. Mordovets, A. Ya. Shul'man, and I. D. Yaroshetskiĭ, Zh. Éksp. Teor. Fiz. **102**, 907 (1992) [Sov. Phys. JETP **75**, 495 (1992)].
[60] I. N. Kotel'nikov, A. Ya. Shul'man, N. A. Mordovets, S. D. Ganichev, and W. Prettl, J. Phys. Low-Dimens. Struct. **12**, 133 (1995).
[61] S. D. Ganichev, A. Ya. Shul'man, N. A. Mordovets, I. N. Kotel'nikov, and W. Prettl, Int. J. Infrared Millim. Waves **17**, 1353 (1996).
[62] I. N. Kotel'nikov, A. Ya. Shul'man, N. A. Varvanin, S. D. Ganichev, B. Mayerhofer, and W. Prettl, JETP Lett. **62**, 48 (1995).
[63] S. D. Ganichev, Ya. V. Terent'ev, and I. D. Yaroshetskiĭ, Pisma Zh. Tekh. Fiz. **11**, 46 (1985) [Sov. Tech. Phys. Lett. **11**, 20 (1985)].
[64] S. D. Ganichev, S. A. Emel'yanov, A. G. Pakhomov, Ya. V. Terent'ev, and I. D. Yaroshetskiĭ, Pisma Zh. Tekh. Fiz. **11**, 913 (1985) [Sov. Tech. Phys. Lett. **11**, 377 (1985)].
[65] A. V. Andrianov, E. V. Beregulin, S. D. Ganichev, K. Yu. Glukh, and I. D. Yaroshetskiĭ, Pisma Zh. Tekh. Fiz. **14**, 1326 (1988) [Sov. Tech. Phys. Lett. **14**, 580 (1988)].
[66] S. D. Ganichev, K. Yu. Glukh, I. N. Kotel'nikov, N. A. Mordovets, A. Ya. Shul'man, and I. D. Yaroshetskiĭ, Pis'ma Zh. Tekh. Fiz. **15**, No. 8, 8 (1989) [Sov. Tech. Phys. Lett. **15**, 582 (1989)].
[67] E. V. Beregulin, S. D. Ganichev, I. D. Yaroshetskiĭ, P. T. Lang, W. Schatz, and K. F. Renk, *Phys. Concepts of Materials for Novel Opto-Electronic Device Applications II: Device Physics and Applications*, Proc. SPIE **1362**, 853 (1990).
[68] E. V. Beregulin, S. D. Ganichev, and I. D. Yaroshetskiĭ, *Physical Concepts of Materials for Novel Opto-Electronic Device Applications II*, edited by F. Bertran and E. Gornik, Proc. SPIE **1985**, 523 (1993).
[69] S. D. Ganichev, W. Prettl, and P. G. Huggard, Phys. Rev. Lett. **71**, 3882 (1993).
[70] S. M. Ryvkin, *Photoelectric Phenomena in Semiconductors* [in Russian], Fizmatgiz, Moscow, 1963.
[71] G. M. Martin and S. Makram-Ebeid, in *Deep Centers in Semiconductors*, edited by S. T. Pantelides (Gordon and Breach, N.Y., 1986).
[72] N. T. Bagraev and V. A. Mashkov, Izv. Akad. Nauk SSSR, Ser. Fiz **50**, 251 (1986) [*sic*].
[73] D. J. Chadi and K. J. Chang, Phys. Rev. B **39**, 10063 (1989).
[74] P. M. Mooney, J. Appl. Phys. **67**, R1 (1990).
[75] V. N. Abakumov, V. I. Perel, and I. N. Yassievich, *Nonradiative Recombination in Semiconductors*, edited by V. M. Agranovich and A. A. Maradudin, *Modern Problems in Condensed Matter Sciences*, Vol. 33 (North-Holland, Amsterdam, 1991).
[76] P. M. Mooney and T. N. Theis, Comments Condens. Matter Phys. **16**, 167 (1992).
[77] R. C. Newman, Semicond. Sci. Technol. **9**, 1749 (1994).
[78] K. Huang and A. Rhys, Proc. R. Soc. London, Ser. A **204**, 406 (1950).
[79] C. H. Henry and D. V. Lang, Phys. Rev. B **15**, 989 (1977).
[80] C. H. Henry and D. V. Lang, Phys. Rev. B **15**, 989 (1975).
[81] T. Markvart, J. Phys. C **17**, 6303 (1984).
[82] V. N. Abakumov, I. A. Merkulov, V. I. Perel', and I. N. Yassievich, Zh. Éksp. Teor. Fiz. **89**, 1472 (1985) [Sov. Phys. JETP **62**, 853 (1985)].
[83] P. T. Landsberg, *Recombination in Semiconductors* (Cambridge University Press, New York, 1991).
[84] L. D. Landau and E. M. Lifshits, *Quantum Mechanics* (Pergamon Press, Oxford, 1974).
[85] R. Landauer and Th. Martin, Rev. Mod. Phys. **66**, 217 (1994).
[86] S. D. Ganichev, I. N. Yassievich, and W. Prettl, Semicond. Sci. Technol. **11**, 679 (1996).
[87] L. V. Keldysh, Zh. Éksp. Teor. Fiz. **34**, 994 (1958) [Sov. Phys. JETP **7**, 685 (1958)].
[88] S. Makram-Ebeid and M. Lannoo, Phys. Rev. B **25**, 6406 (1982).
[89] V. Karpus and V. I. Perel', JETP Lett. **42**, 497 (1985).
[90] V. Karpus and V. I. Perel, Zh. Éksp. Teor. Fiz. **91**, 2319 (1986) [Sov. Phys. JETP **64**, 1376 (1986)].
[91] A. F. Tasch, Jr., and C. T. Sah, Phys. Rev. B **1**, 800 (1970).
[92] K. Irmscher, H. Klose, and K. Maass, Phys. Status Solidi A **75**, K25 (1983).
[93] V. Karpus, JETP Lett. **44**, 430 (1986).
[94] J. Frenkel, Phys. Rev. **54**, 647 (1938).
[95] V. N. Abakumov, V. Karpus, V. I. Perel', and I. N. Yassievich, Fiz. Tekh. Poluprovodn. **22**, 262 (1988) [Sov. Phys. Semicond. **22**, 159 (1988)].
[96] L. V. Keldysh, Zh. Éksp. Teor. Fiz. **47**, 1945 (1964) [Sov. Phys. JETP **20**, 1307 (1965)].
[97] Yu. A. Bychkov and A. M. Dykhne, Zh. Éksp. Teor. Fiz. **58**, 1734 (1970) [Sov. Phys. JETP **31**, 928 (1970)].
[98] B. I. Ivlev and V. I. Mel'nikov, Zh. Éksp. Teor. Fiz. **90**, 2208 (1986) [Sov. Phys. JETP **63**, 1295 (1986)].
[99] A. A. Vedenov, G. D. Myl'nikov, and D. N. Sobolenko, Usp. Fiz. Nauk **138**, 477 (1982) [Sov. Phys. Usp. **25**, 833 (1982)].
[100] M. Rosenbluth, R. J. Temkin, and K. J. Button, Appl. Opt. **15**, 2635 (1976).
[101] S. F. Dyubko and L. D. Fesenko, *Tables of Lasing Lines of Optically-Pumped Submillimeter Lasers* [in Russian] (Preprint IRE, Acad. Sci. Ukr. SSR, Kharkov, 1979).
[102] O. J. E. Knight, NPL Report **45**, 200 (1981).

[103] K. Gullberg, B. Hartmann, and B. Kleman, Phys. Scr. **8**, 177 (1973).
[104] C. T. Gross, J. Kiess, A. Mayer, and F. Keilmann, IEEE J. Quantum Electron. **QE-23**, 377 (1987).
[105] B. K. Meyer, G. Bischopink, K. W. Benz, A. Schäfner, and G. Pensl, J. Cryst. Growth **128**, 475 (1993).
[106] R. Krause-Rehberg, Th. Drost, A. Polity, G. Roos, G. Pensl, D. Volm, B. K. Meyer, G. Bischopink, and K. W. Benz, Phys. Rev. B **48**, 11723 (1993).
[107] R. J. Keyes, *Optical and Infrared Detectors, Topics in Applied Physics* (Springer, Berlin, 1980).
[108] S. D. Ganichev, J. Diener, and W. Prettl, Solid State Commun. **92**, 883 (1994).
[109] S. D. Ganichev, J. Diener, I. N. Yassievich, and W. Prettl, Europhys. Lett. **29**, 315 (1995).
[110] S. D. Ganichev, I. N. Yassievich, W. Prettl, J. Diener, B. K. Meyer, and K. W. Benz, Phys. Rev. Lett. **75**, 1590 (1995).
[111] S. D. Ganichev, E. Ziemann, Th. Gleim, I. N. Yassievich, and W. Prettl, Verh. Dtsch. Phys. Ges. **5**, 700 (1997).
[112] E. V. Buryak, S. A. Kaufman, and K. M. Kulikov, Fiz. Tverd. Tela (Leningrad) **5**, 345 (1963) [Sov. Phys. Solid State **5**, 249 (1963)].
[113] S. A. Kaufman, K. M. Kulikov, and N. P. Likhtman, Fiz. Tekh. Poluprovodn. **4**, 129 (1970) [Sov. Phys. Semicond. **4**, 102 (1970)].
[114] S. D. Ganichev, S. A. Emel'yanov, and I. D. Yaroshetskiĭ, Fiz. Tekh. Poluprovodn. **21**, 1011 (1987) [Sov. Phys. Semicond. **21**, 618 (1987)].
[115] S. D. Ganichev, J. Diener, and W. Prettl, Appl. Phys. Lett. **64**, 1977 (1994).
[116] I. A. Merkulov, A. A. Pakhomov, and I. N. Yassievich, Fiz. Tverd. Tela (Leningrad) **28**, 2127 (1986) [Sov. Phys. Solid State **28**, 1188 (1986)].
[117] R. Combescot and G. Schreder, J. Phys. C **6**, 1363 (1973).
[118] T. Hirai and O. Nakada, J. Appl. Phys. **7**, 112 (1968).
[119] M. Ieda, G. Sawa, and S. Kato, J. Appl. Phys. **42**, 3737 (1971).
[120] G. A. N. Connell, D. L. Camphausen, and W. Paul, Philos. Mag. **26**, 541 (1972).
[121] D. Pai, J. Appl. Phys. **46**, 5122 (1975).
[122] N. G. Zhdanova, M. S. Kagan, E. G. Landsberg, L. V. Levkin, and V. V. Petrishchev, JETP Lett. **62**, 119 (1995).
[123] R. H. M. Groeneveld and D. Grischovsky, JOSA B **11**, 1 (1994).
[124] D. Grischovsky, S. Kelding, M. van Exter, and C. H. Fattinger, JOSA B **7**, 2006 (1990).
[125] M. S. Sherwin, K. Craig, B. Galdrikian, J. N. Heyman, A. G. Markelz, K. Campman, S. Farfad, P. F. Hopkins, and A. C. Gossard, Physica D **83**, 229 (1995).
[126] B. N. Murdin, C. J. G. M. Langerak, M. Helm, P. Kruck, W. Heiss, V. Rosskopf, G. Strasser, E. Gornik, M. Dür, S. M. Goodnick, S. C. Lee, I. Galbraith, and C. R. Pidgeon, Superlattices Microstruct. **19**, 17 (1996).
[127] S. D. Ganichev, E. Zepezauer, W. Raab, I. N. Yassievich, and W. Prettl, Phys. Rev. B **55**, 9243 (1997).
[128] I. V. Altukhov, Ya. E. Pokrovskiĭ, O. I. Smirnova, and V. P. Sinis, Fiz. Tekh. Poluprovodn. **24**, 1134 (1990) [Sov. Phys. Semicond. **24**, 450 (1990)].
[129] Ya. E. Pokrovskii, O. I. Smirnova, and N. A. Khvalkovskii, Solid State Commun. **93**, 405 (1995).
[130] R. Z. Bachrach, P. D. Dapkus, and O. G. Lorimor, J. Appl. Phys. **45**, 4971 (1974).
[131] A. N. Pikhtin, D. A. Yas'kov, and G. F. Glinskiĭ, Fiz. Tverd. Tela (Leningrad) **12**, 386 (1970) [Sov. Phys. Solid State **12**, 307 (1970)].
[132] D. N. Nasledov, V. V. Negreskul, S. I. Radautsan, and S. V. Slobodchikov, Phys. Status Solidi **10**, 37 (1965).
[133] H. C. Montgomery, J. Appl. Phys. **39**, 2002 (1968).
[134] P. Dean, in *Deep Centers in Semiconductors* (Gordon and Breach, N.Y., 1986).
[135] W. Scott, J. Appl. Phys. **50**, 472 (1979).
[136] K. Seeger, *Semiconductor Physics* (Springer, Wien, 1973) [Russian trans., Mir, Moscow, 1977].
[137] V. Denis and J. Pazhela, *Hot Electrons* [in Russian], Mintis, Vilnjus, 1971.
[138] *Electrons in Semiconductors*, edited by J. Pozhela, **3**, (Mokslas, Vilnjus, 1981).
[139] M. Asche, Z. S. Gribnikov, V. V. Mitin, and O. G. Sarbeĭ, *Hot Electrons in Many-Valley Semiconductors* [in Russian] Naukova Dumka, Kiev, 1982.
[140] E. M. Conwell, *High-Field Transport in Semiconductors* (Academic Press, New York, 1967) [Russian trans., Mir, Moscow, 1970).
[141] I. N. Yassievich and I. D. Yaroshetskiĭ, Fiz. Tekh. Poluprovodn. **9**, 857 (1975) [Sov. Phys. Semicond. **9**, 565 (1975)].
[142] V. G. Agafonov, P. M. Valov, B. S. Ryvkin, and I. D. Yaroshetskiĭ, Fiz. Tekh. Poluprovodn. **9**, 867 (1975) [Sov. Phys. Semicond. **9**, 571 (1975)].
[143] J. B. Gunn, J. Phys. Chem. Solids **8**, 239 (1959).

Translated by G. Skrebtsov